Journal of
Medicinal Chemistry

Article

Discovery of Novel Dual Poly(ADP-ribose)polymerase (PARP) and Phosphoinositide 3-kinase (PI3K) Inhibitors as A Promising Strategy for Cancer Therapy

Junwei Wang, Hui Li, Guangchao He, Zhaoxing Chu, Kewen Peng, Yiran Ge, Qihua Zhu, and Yungen Xu

J. Med. Chem., **Just Accepted Manuscript** • DOI: 10.1021/acs.jmedchem.9b00622 • Publication Date (Web): 17 Dec 2019

Just Accepted

is published by the American Chemical Society. 1155 Sixteenth Street N.W., Washington, DC 20036

Discovery of Novel Dual Poly(ADP-ribose)polymerase (PARP) and Phosphoinositide 3-kinase (PI3K) Inhibitors as A Promising Strategy for Cancer Therapy

Junwei Wang[a], Hui Li[a], Guangchao He[b], Zhaoxing Chu[b], Kewen Peng[b], Yiran Ge[b], Qihua Zhu*[a,b] and Yungen Xu*[a,b]

[a]State Key Laboratory of Natural Medicines, China Pharmaceutical University, Nanjing, 210009, China

[b]Jiangsu Key Laboratory of Drug Design and Optimization, Department of Medicinal Chemistry, China Pharmaceutical University, Nanjing 210009, China

Abstract: Concomitant inhibition of PARP and PI3K pathways has been recognized as a promising strategy for cancer therapy, which may expand the clinical utility of PARP inhibitors. Herein, we report the discovery of dual PARP/PI3K inhibitors that merge the pharmacophores of PARP and PI3K inhibitors. Among them, compound **15** stands out as the most promising candidate with potent inhibitory activities against both PARP-1/2 and PI3Kα/δ with pIC_{50} values greater than 8. Compound **15** displayed superior anti-proliferative profiles against both BRCA-deficient and BRCA-proficient cancer cells in cellular assays. The prominent synergistic effects produced by the concomitant inhibition of the two targets were elucidated by comprehensive biochemical and cellular mechanistic studies. In vivo, **15** showed more efficacious anti-tumor activity than the corresponding drug combination (Olaparib + BKM120) in MDA-MB-468 xenograft model with a tumor growth inhibitory rate of 73.4% without causing observable toxic effects. All the results indicate that **15**, a first potent dual PARP/PI3K inhibitor, is a highly effective anticancer compound.

Keywords: PARP inhibitor; PI3K inhibitor; dual PARP/PI3K inhibitors; synergistic effects.

INTRODUCTION

In the context of cancer, single-agent/single-target therapeutics are poorly effective due to the complexity of cancer pathways and the emergence of drug resistance.[1] Consequently, combination therapies targeting two or more pathways constitute the mainstays of modern cancer treatment.[2] However, combination therapies are hampered by their complicated pharmacokinetics, intricate toxicity profiles, undesirable drug-drug interactions, as well as poor patient compliance. Moreover, expensive and time-consuming clinical research pertaining to drug combination presents yet another great obstacle for the application of combination therapies against cancers.[3-6] In an effort to circumvent the limitations of combination regimens, we have focused on the development of dual inhibitors capable of blocking two classes of enzymes simultaneously. Amid the numerous enzyme targets, we found poly(ADP-ribose)polymerases (PARPs) and phosphoinositide 3-kinases (PI3Ks) are two particularly suitable targets for our endeavor to develop dual inhibitors against BRCA-proficient cancers.

PARPs are a family of enzymes that catalyze the transfer of ADP-ribose from nicotinamide adenine dinucleotide (NAD^+) onto acceptor proteins.[7,8] PARP-1 is the most abundant and well-studied member of this family, which plays a crucial role in the repair of DNA single-strand breaks (SSBs).[9,10] The role of PARP-1 in DNA repair has made it a highly pursued therapeutic target for cancer treatment, which prompted the development of numerous PARP-1 inhibitors.[11-13] PARP inhibitors were initially developed as chemo- or radio-sensitizing agents by inhibiting DNA damage repair and promoting apoptosis of tumor cells.[14] In 2005, two groups described the synthetic lethality (SL) between PARP inhibition and BRCA1/2 mutations, suggesting a novel strategy for treating patients with BRCA-mutant tumors.[15,16] Therefore, beyond their use as chemosensitizers,

PARP inhibitors are also promising monotherapy agents for patients with BRCA1/2 mutations.[17,18] To date, four PARP inhibitors, Olaparib[19], Rucaparib[20], Niraparib[21] and Talazoparib[22] have been approved by the FDA or EMA for the treatment of BRCA-mutant advanced ovarian and breast cancers. In addition, a number of other PARP inhibitors, such as Veliparib[23], are in clinical evaluation for cancer therapies.[24,25] However, clinical development of PAPR inhibitors has been severely hampered by their narrow indication spectrum entailed by SL. Thus, only a small subgroup of patients with BRCA1/2 mutations can benefit from this therapy, posing a great limitation on the utility of PARP inhibitors.[18]

The PI3K/AKT/mTOR pathway is a major signaling cascade implicated in cancer, and PI3K is a well-established target for anticancer therapy.[26,27] It was reported that PI3K plays a key regulatory role in stabilizing and preserving DNA double-strand break (DSB) repair by interacting with the homologous recombination (HR) complex.[28,29] In 2012, Ibrahim and Juvekar groups independently found that PI3K inhibition promotes HR deficiency by downregulating BRCA1/2 and sensitizes BRCA-proficient tumors to PARP inhibition, which provides a rationale for the combined administration of PI3K and PARP inhibitors to expand the utility of PARP inhibitors beyond BRCA1/2-mutant cancers.[30,31] On the basis of these findings, a clinical trial of the combination therapy of BKM120 and Olaparib has been initiated in patients with recurrent triple-negative breast cancer (TNBC) and high-grade serous ovarian cancer.[32]

Such ground-breaking research encouraged us to develop small-molecule inhibitors concomitantly targeting PARP and PI3K, given that no dual PARP/ PI3K inhibitors are currently available in clinic or in the market. However, developing pharmacologically attractive dual PARP/PI3K inhibitors is difficult, and the challenges include: retaining high potency and specificity

simultaneously for the two targets within a single molecule; striking an appropriate balance in targeting PARP and PI3K; and controlling the size and polarity of such hybrid compounds for a favorable physiochemical and pharmacologic profile.

Herein, we present the design, synthesis and biological evaluation of dual PARP/PI3K inhibitors. Our data of the most promising compound **15** indicate that it can produce pronounced synergistic anti-cancer effects and is more efficacious than the corresponding combination therapy consisting of Olaparib and BKM120.

DESIGN OF DUAL INHIBITORS

Structures of Olaparib (PARP inhibitor) and BKM120 (PI3K inhibitor)[33] served as the starting point for our endeavor to design dual PARP/PI3K inhibitors. Analysis of the reported Olaparib-PARP-1 complexes revealed that the phthalazine moiety is critical, since it binds to the catalytic domain of PARP. However, the cyclopropanecarbonyl group (black section of Olaparib in Figure 1A) is not necessary for PARP inhibition since it extends out toward solvent, thus, structural modifications can be tolerated in this region.[34-37] On the other hand, scrutiny of the BKM120-PI3K binding mode revealed that the morpholine group (black section of BKM120 in Figure 1) does not interact with the ATP-binding region and thus we can replace it with a linker to incorporate the pharmacophores of PARP inhibitors.[33,38] Based on these observations, we designed a series of potential dual PARP/PI3K inhibitors **1-18** by combining the red section of Olaparib with the blue section of BKM120 through a linker, as shown in Figure 1.

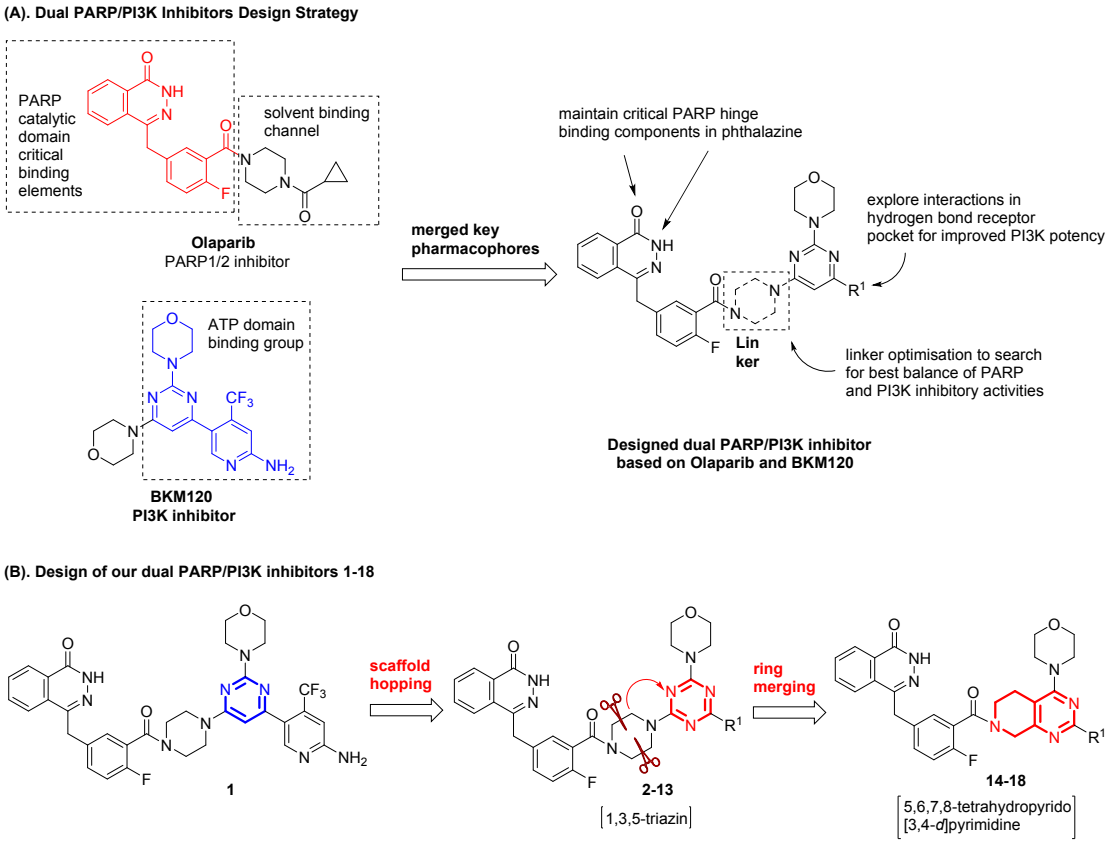

Figure 1. Schematic showing design of a merged PARP-PI3K pharmacophore taking advantage of PARP catalytic domain critical binding group and PI3K ATP domain binding group

Firstly, we chose the piperazine moiety of Olaparib as the linker to bridge the two structural sections descried above, since this strategy appeared to be the most synthetically feasible one (Figure 1B). To justify the rationale of this design strategy, a docking study was carried out to probe the binding mode of **1** toward both PARP-1 (PDB code 5DS3)[34] and PI3Kα (PDB code 4JPS)[39]. The docked pose into the PARP-1 active site showed that compound **1** can form three key hydrogen bonds with Ser904 and Gly863, and π-stacking interactions with Tyr896 and Tyr907. The docking model in the PI3Kα active site showed that compound **1** can form a hydrogen bond with Val851 and two key hydrogen bonds with Asp810 and Asp933 (Figure 2). Thus, it can be concluded that compound **1** fits in the active sites of PARP-1 and PI3Kα in a fashion similar to Olaparib and BKM120, respectively, which indicates that compound **1** has the potential to inhibit the activities

of both PARP-1 and PI3Kα.

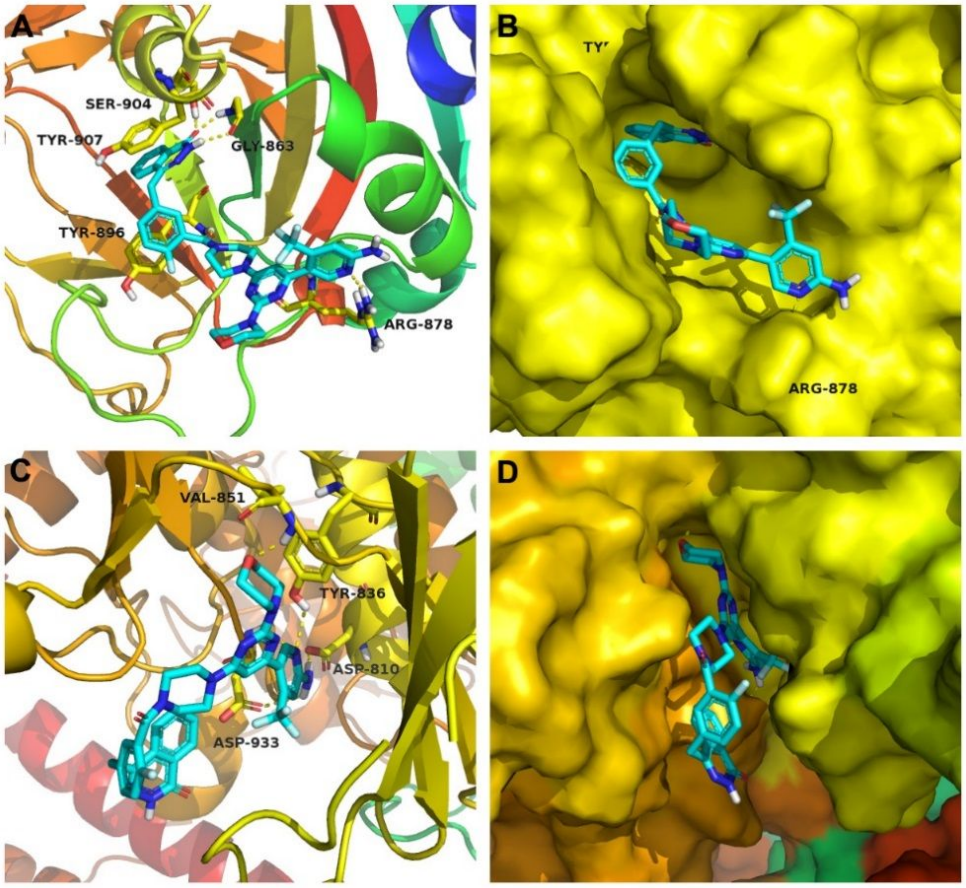

Figure 2. Docking studies of compound **1** with PARP-1 (5DS3) and PI3Kα (4JPS). Representation of the predicted binding mode of compound **1** in the active site of PARP-1 (A, B) and PI3Kα (C, D). Hydrogen bonds are represented as yellow dotted lines. For clarity, nonpolar H atoms are not represented.

RESULTS AND DISCUSSION

Structure Optimization and In Vitro PARP-1/PI3Kα Inhibition Assay.

Inspired by the docking results, we synthesized compound **1** and evaluated it for PARP-1 and PI3Kα inhibitory activities in vitro. The results showed that compound **1** has good PARP-1 and PI3Kα inhibitory activities with pIC_{50} values of 7.81 and 6.49, respectively. Although there is some imbalance in its activities against the two enzymes, compound **1** is an appropriate lead compound deserving further optimization.

In our efforts to improve the PI3K inhibitory activity of **1**, the pyrimidine scaffold was first replaced by 1,3,5-triazine, leading to compound **2**. Notably, the inhibitory activities of compound **2** against PARP-1 and PI3Kα both increased with pIC_{50} values of 8.02 and 6.77, respectively (Table 1). This result showed that the 1,3,5-triazine moiety is beneficial for both PARP and PI3K inhibition. Consequently, we retained this 1,3,5-triazine moiety in further modifications. The reported structure-activity relationships (SARs) of PI3K inhibitors suggest that modification of the R^1 substituent serving as a hydrogen-bond donor may lead to an improved PI3K inhibitory activity.[33,40,41] Thus, we designed different aromatic moieties to replace the 2-amino-4-(trifluoromethyl)-5-pyridinyl. Eleven compounds (**3-13**) were synthesized and evaluated for PARP-1 and PI3Kα inhibitory activities. As expected, the change in R^1 substituent brought about little effect on PARP-1 inhibitory activity; compounds **3-13** all exhibited excellent PARP-1 inhibitory activity in the low nanomolar range, as shown in Table 1. However, the inhibition of PI3Kα varied considerably depending on the R^1 substituent. The aromatic groups with a lower electron density showed better PI3Kα inhibitory activity; for example, pyrimidine (pIC_{50}: 7.04) and pyridine (pIC_{50}: 6.88) rings were better than benzene (pIC_{50}: 6.48), indazole (pIC_{50}: 6.46) and indole (pIC_{50}: 6.20) rings. The position of the substituents on the ring also influences the activity; for example, compound **2**, bearing a trifluoromethyl at the para-position, showed stronger PI3Kα inhibitory activity (pIC_{50}: 6.77) than compound **3** (pIC_{50}: 5.92) which bears a trifluoromethyl at the meta-position. Nonetheless, the PI3Kα inhibitory activities of compounds **3-13** were much weaker than BKM120, and only compound **4** displayed moderate PI3Kα inhibitory activity with pIC_{50} of 7.04. Therefore, the first round of structural optimization culminated in compound **4** that displayed acceptable PARP-1 and PI3Kα inhibitory activities with pIC_{50} values of 9.08 and 7.04, respectively.

Although the PARP-1 inhibitory activity is comparable to Olaparib and the PI3Kα inhibitory activity is only 3.5-fold less potent than BKM120, there is a 120-fold difference in the inhibitory activity between PARP-1 and PI3Kα. Thus, further structural optimization efforts are needed to strike an appropriate inhibitory balance between PARP-1 and PI3Kα.

Table 1. In Vitro PARP-1 and PI3Kα Inhibitory Activities of Compounds 2-13

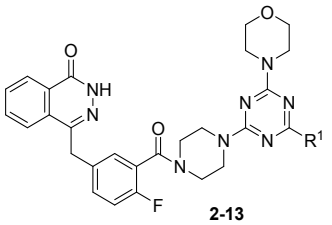

2-13

Compd	R^1	pIC_{50}[a]	
		PARP-1	PI3Kα
2	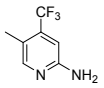	8.02±0.06	6.77±0.07
3	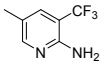	8.95±0.09	5.92±0.12
4	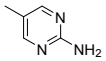	9.08±0.06	7.04±0.09
5	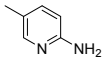	8.97±0.07	6.88±0.12
6	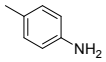	8.93±0.06	6.48±0.09
7	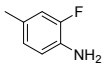	9.08±0.08	6.25±0.13
8	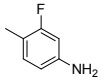	9.14±0.05	6.15±0.06
9	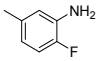	8.96±0.05	5.64±0.09
10		9.36±0.09	6.46±0.08
11		9.17±0.13	< 5
12		9.19±0.16	6.20±0.06
13		9.16±0.07	6.16±0.14

Olaparib	9.08±0.06	ND[b]
BKM120	ND[b]	7.61±0.05

[a]pIC_{50} values for enzymatic inhibition of PARP-1 and PI3Kα; data are expressed as the mean ± SD from the dose-response curves of three independent experiments. [b]ND, not detected.

It was observed that section A of compound **4** was crucial for the maintenance of PARP-1 inhibitory activity, while the morpholine and aromatic amine moieties were necessary for PI3Kα inhibitory activity (Figure 3). Thus, only the piperazine linker can be modified. Via scaffold hopping, we modified the linker of compound **4** by merging the pyrimidine and piperazine components into a bicyclic system (Figure 3). Unexpectedly, the newly designed compound **14** not only exhibited excellent PARP-1 and PI3Kα inhibitory activities with pIC_{50} values of 8.59 and 8.32, respectively, but also struck an inhibitory balance between the two targets (Table 2).

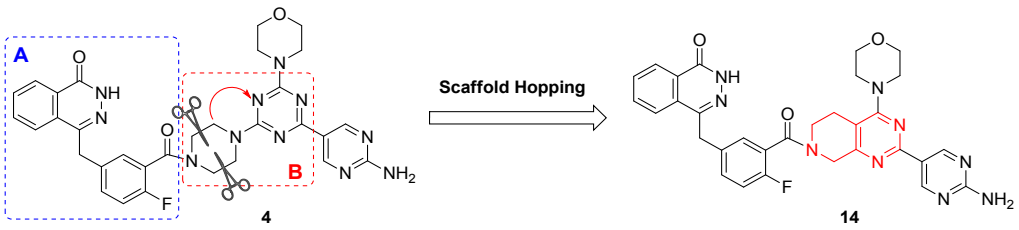

Figure 3. Further compound design and structure optimization

Encouraged by this result, we kept the tetrahydropyrido[3,4-d]pyrimidine scaffold while replacing the R^1 substituent of **14**, leading to compounds **15-18**. The inhibitory activities of the newly designed compounds are listed in Table 2. To our disappointment, although all the compounds maintained high PARP-1 inhibitory activity in the low nanomolar range (pIC_{50}: 8.10-8.59), the PI3Kα inhibitory activities of compounds **16-18** reduced considerably. As a result, the third round of structural optimization culminated in compounds **14** and **15**, which remained potent

and well-balanced dual PARP-1/PI3Kα inhibitory activities with pIC_{50} values of 8.59/8.22 and 8.32/8.25, respectively.

Table 2. In Vitro PARP-1 and PI3Kα Inhibitory Activities of Compounds 14-18

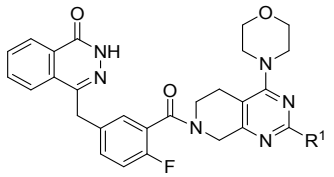

14-18

Compd	R^1	pIC_{50}[a]	
		PARP-1	PI3Kα
14		8.59±0.15	8.32±0.16
15		8.22±0.06	8.25±0.09
16		8.10±0.11	7.52±0.08
17		8.21±0.07	7.35±0.09
18		8.31±0.08	7.36±0.08

[a]pIC_{50} values for enzymatic inhibition of PARP-1 and PI3Kα; data are expressed as the mean ± SD from the dose-response curves of three independent experiments.

In Vitro Anti-proliferation Assay.

Considering their prominent enzymatic inhibitory activities, we then preliminarily screened compounds **14** and **15** in cellular assays using HCC1937 (BRCA1-deficient breast cancer cells), HCT116 (BRCA2-deficient colorectal cancer cells), MDA-MB-231 and MDA-MB-468 cancer cell lines (BRCA-proficient triple-negative breast cancer cells). As demonstrated in Table 3, Olaparib showed strong anti-proliferative activity against BRCA-deficient cells, but weak inhibitory activity against BRCA-proficient cells. In contrast, compounds **14** and **15** not only showed significant

inhibitory activity against BRCA-deficient cells HCC1937 and HCT116, but also displayed potent anti-proliferative activity against BRCA-proficient cells MDA-MB-231 and MDA-MB-468. In addition, the anti-proliferative activities of compound **15** against these cancer cells are at least four times more potent than BKM120.

Table 3. In Vitro Growth-Inhibitory Activities of Compounds 14 and 15

Compd	pIC_{50}			
	HCT116	HCC1937	MDA-MB-231	MDA-MB-468
14	5.80±0.06	5.46±0.16	5.45±0.05	5.59±0.01
15	6.06±0.08	5.98±0.40	6.00±0.17	6.01±0.15
Olaparib	5.52±0.08	5.34±0.03	4.74±0.09	4.86±0.11
BKM120	5.44±0.07	5.20±0.06	5.22±0.05	5.40±0.04
Olaparib+BKM120	5.91±0.10	5.77±0.05	5.80±0.05	5.89±0.23

To explore whether the applications of dual PARP/PI3K inhibitors could be further extended to other BRCA-proficient cancer cell lines, we evaluated compound **15** for its anti-proliferative activity against a panel of eight other BRCA-proficient cell lines that represent different tumor types including breast cancer, ovarian cancer, colorectal cancer, pancreatic cancer, prostate cancer, non-small cell lung cancer, kidney cancer, lymphoma and leukemia. It is noteworthy that, compared with Olaparib and BKM120, compound **15** exhibited considerably more potent in vitro antitumor activity against most of these BRCA-proficient cancer cells (Table 4). The potency of **15** against various tumor cell lines demonstrates its therapeutic potential in BRCA-mutant cancers that typically circumscribe the application of traditional PARP inhibitors.

Table 4. In Vitro Growth-Inhibitory Activities of 15 in Various Cancer Cell Lines

Cell lines	Cell type	pIC_{50}

		15	Olaparib	BKM120	Olaparib+ BKM120
BxPC-3	pancreatic cancer	5.97±0.06	4.93±0.14	5.39±0.05	5.61±0.07
A2780	ovarian cancer	6.40±0.06	6.13±0.11	6.38±0.09	6.46±0.08
Jurkat	leukemia	6.03±0.01	5.77±0.04	5.85±0.07	5.89±0.06
DU145	prostate cancer	6.05±0.06	5.20±0.13	5.42±0.08	5.93±0.05
A549	lung cancer	6.27±0.06	5.27±0.06	5.77±0.06	6.19±0.02
Caki-1	kidney cancer	6.02±0.04	5.15±0.05	5.56±0.03	5.73±0.05
Ramos	lymphoma	5.97±0.16	5.40±0.13	5.44±0.06	5.93±0.13
SW620	colorectal cancer	5.55±0.18	4.99±0.12	5.29±0.18	5.49±0.05

Cellular Mechanism of Action Studies.

1. Western Blot Analysis of Protein Expression in Vitro

Cellular mechanistic studies of **14** and **15** were carried out to explain their superior anti-proliferative profiles against BRCA-proficient cancer cells. Firstly, western blot analysis was conducted to explore whether compounds **14** and **15** affect PARP's activity and disturb the PI3K pathway in exerting their anti-proliferative effects. As shown in Figure 4, the autophosphorylation levels of AKT and S6 reduced while the autophosphorylation level of ERK increased after treating cells with compounds **14** and **15**, indicating that they can inhibit the PI3K pathway and activate the ERK pathway. In addition, cell apoptosis was pronounced given the significantly elevated cleaved PARP level observed after the treatment of **14** or **15**, suggesting these two compounds severely jeopardized the DNA-repairing functions of PARP.

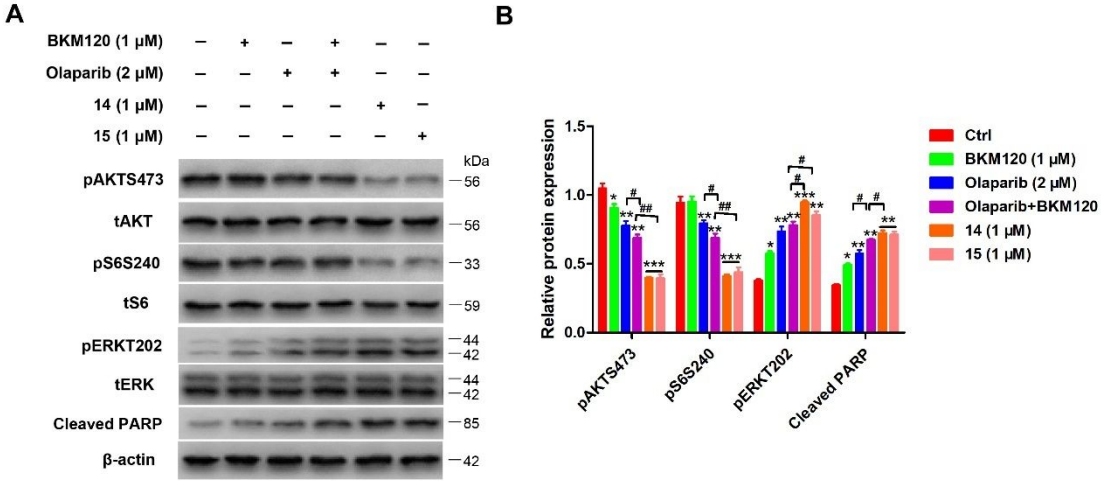

Figure 4. Effects of BKM120, Olaparib, BKM120 (1 μM) + Olaparib (2 μM), compounds **14** and **15** on protein expression of MDA-MB-468 cancer cells. Western blot analysis of proteins (pAKT, pS6S240, pERK and cleaved PARP) as indicated in MDA-MB-468 cancer cells treated with the indicated compounds for 72 h. β-actin was used as a loading control. The data are shown as the mean ± SD of three independent experiments. *$p < 0.05$ *vs.* control, **$p < 0.01$, ***$p < 0.001$; $^{\#}p < 0.05$, $^{\#\#}p < 0.01$, $^{\#\#\#}p < 0.001$.

2. Quantitative Real-Time PCR

To verify whether BRCA1/2 was downregulated in MDA-MB-468 cancer cells treated with compounds **14** and **15**, the expression of BRCA1/2 at the mRNA level was measured by real-time PCR. As shown in Figure 5, compounds **14** and **15** both displayed a much stronger capability to downregulate the expression of BRCA1/2 at the mRNA level than Olaparib, BKM120 and their combination, suggesting that compounds **14** and **15** probably induced HR deficiency through the downregulation of BRCA1/2.

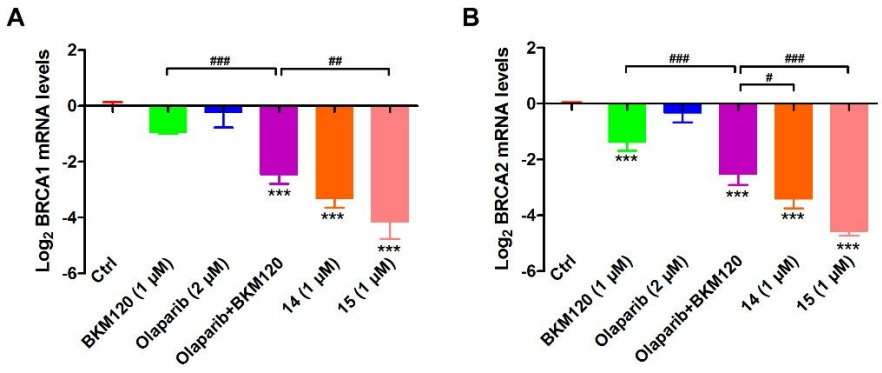

Figure 5. Effects of BKM120, Olaparib, BKM120 (1 μM) + Olaparib (2 μM), compounds **14** and **15** on BRCA1 and BRCA2 expression in MDA-MB-468 cells. Real-time PCR analysis of BRCA1 and BRCA2 expression in MDA-MB-468 cancer cells treated with the indicated compounds. Gene expression was normalized to GAPDH. The data are shown as the mean ± SD of three independent experiments. ***$p < 0.001$ *vs.* control; $^{\#}p < 0.05$, $^{\#\#}p < 0.01$, $^{\#\#\#}p < 0.001$.

3. Immunofluorescence staining analysis of RAD51 and γH2AX

Next, immunofluorescence staining analysis of the RAD51 protein, a marker for the competency of HR repair, was conducted to further confirm the above observations. As shown in Figure 6A, compared with Olaparib, BKM120 and their combination, compounds **14** and **15** significantly reduced the formation of RAD51 foci, indicating impaired HR repair efficiency. Furthermore, it was also observed that the nuclear foci of γH2AX, a biological marker for DSBs, increased significantly after the treatment of compounds **14** and **15** (Figure 6B).

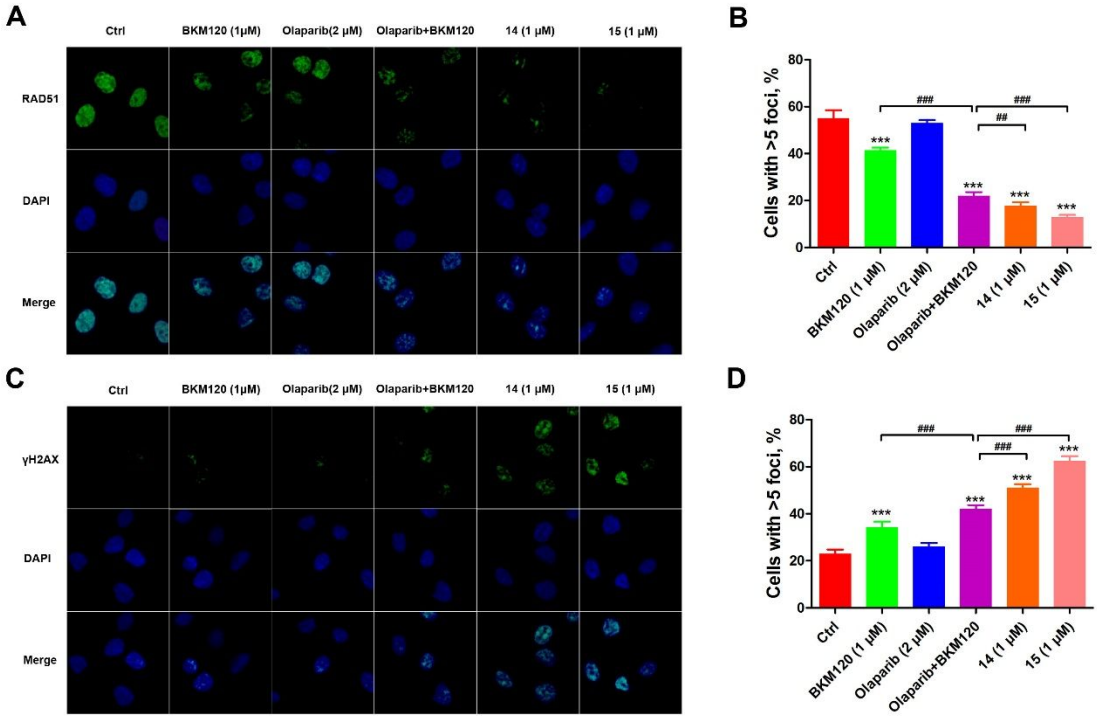

Figure 6. (A) Effects of BKM120, Olaparib, BKM120 (1 μM) + Olaparib (2 μM), compounds **14** and **15** on RAD51 expression in MDA-MB-468 cells. (B) Effects of BKM120, Olaparib, BKM120 (1 μM) + Olaparib (2 μM), compounds **14** and **15** on γH2AX expression in MDA-MB-468 cells. Representative images of immunofluorescence staining of RAD51 and γH2AX in MDA-MB-468 cancer cells treated as indicated for 72 h. Cell nuclei were stained with DAPI. The data are shown as the mean ± SD of three independent experiments. ***$p < 0.001$ *vs.* control; $^{\#\#}p < 0.01$, $^{\#\#\#}p < 0.001$.

4. Comet assay

To gain more insights into the therapeutic effect of the dual PARP/PI3K inhibitors, a comet assay was conducted to evaluate the extent of DNA damage induced. As shown in Figure 7, both compounds **14** and **15** induced large amounts of DNA damage. Notably, compound **15** generated a much higher tail intensity compared with Olaparib, BKM120 or their combination, suggesting its superiority in incurring DNA damage.

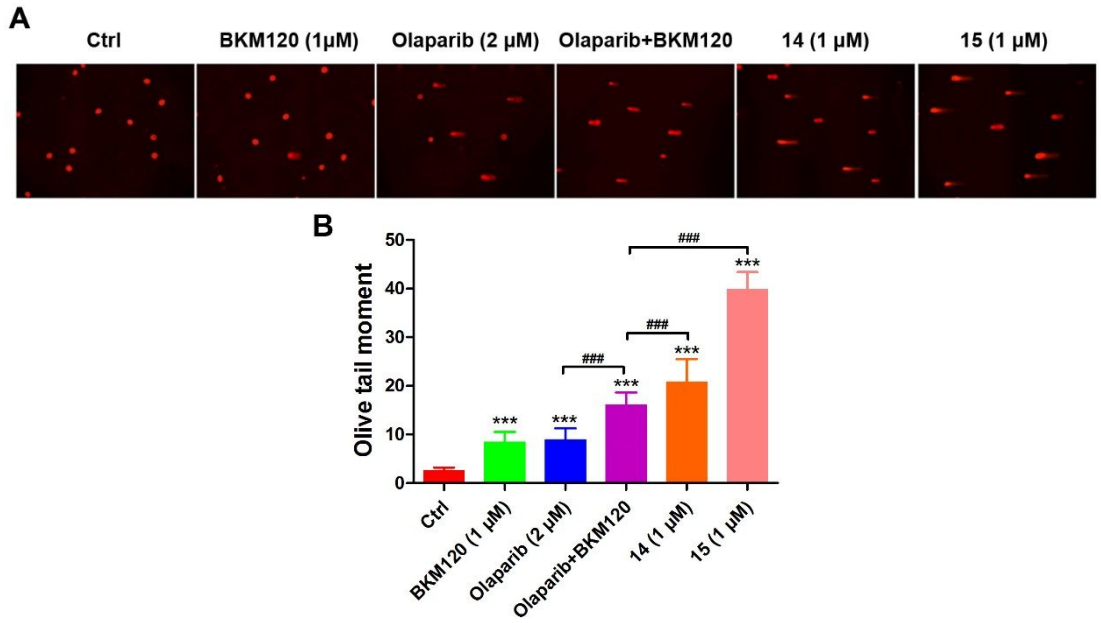

Figure 7. Effects of BKM120, Olaparib, BKM120 (1 μM) + Olaparib (2 μM), compounds **14** and **15** on the DNA damage response in MDA-MB-468 cells. (A) The MDA-MB-468 cancer cells were treated with the indicated compound as single agents or in combination for 72 h. Comet images ×200 taken by fluorescence microscope are shown. (B) The quantitative analysis was performed with the comet analysis software CASP, and the olive tail moment was employed to evaluate DNA damage. The data are shown as the mean ± SD of three independent experiments. $^{***}p < 0.001$ *vs.* control; $^{\#\#\#}p < 0.001$.

5. Apoptosis Analysis

Finally, to determine the effects of compounds **14** and **15** on cell death, we conducted an apoptosis assay using Annexin-V by FACS analysis in the MDA-MB-468 cell line. As shown in Figure 8, compounds **14** and **15** led to a significant increase in cell apoptosis compared with both single-agent treatments and the combination of Olaparib and BKM120. These results suggest that the PI3K inhibition mediated by **14** and **15** can be exploited to induce HR deficiency and thus enhance the sensitivity of BRCA-proficient triple-negative breast cancer cells to PARP inhibition.

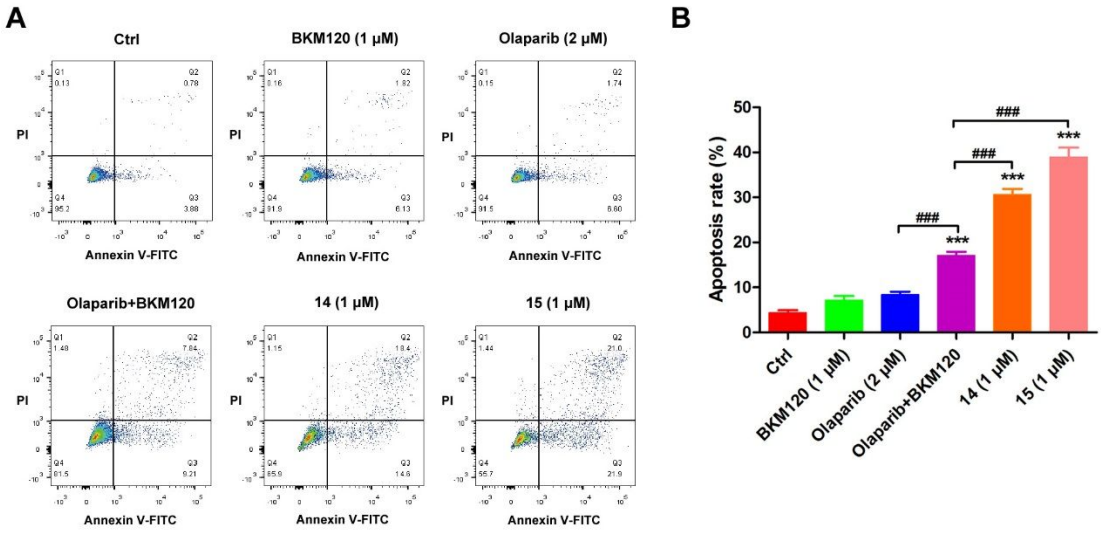

Figure 8. Effects of BKM120, Olaparib, BKM120 (1 μM) + Olaparib (2 μM), compounds **14** and **15** to induce apoptosis of MDA-MB-468 cells. (A) MDA-MB-468 cells were treated with the indicated concentrations of compounds for 72 h. The apoptosis rate was measured using flow cytometry. (B) The percentage of cells in each population. The data are shown as the mean ± SD of three independent experiments. ***$p < 0.001$ *vs.* control; $^{###}p < 0.001$.

In Vivo Antitumor Effects Study.

Based on the excellent enzymatic and antiproliferative activities of compounds **14** and **15** *in vitro*, we then evaluated their antitumor activities *in vivo* in MDA-MB-468 xenograft mouse model. Compounds **14** and **15**, Olaparib, BKM120, and the combination of Olaparib and BKM120 were administered by intraperitoneal injection twice daily (BID) for 34 consecutive days. As shown in Figure 9, compounds **14** and **15** significantly suppressed the tumor growth at a dose of 50 mg·kg^{-1} and they were both well-tolerated with no mortality. The tumor suppression effects of **14** (TGI: 52.7%) and **15** (TGI: 73.4%) were both more effective than Olaparib (TGI: 28.5%) and BKM120 (TGI: 33.4%), and even the combination of Olaparib and BKM120 (TGI: 48.4%). It is also noteworthy that no significant weight fluctuations were observed during the whole process. The results suggest that dual PARP/PI3K inhibitors are superior to the single-target inhibitors in the

antitumor efficacy.

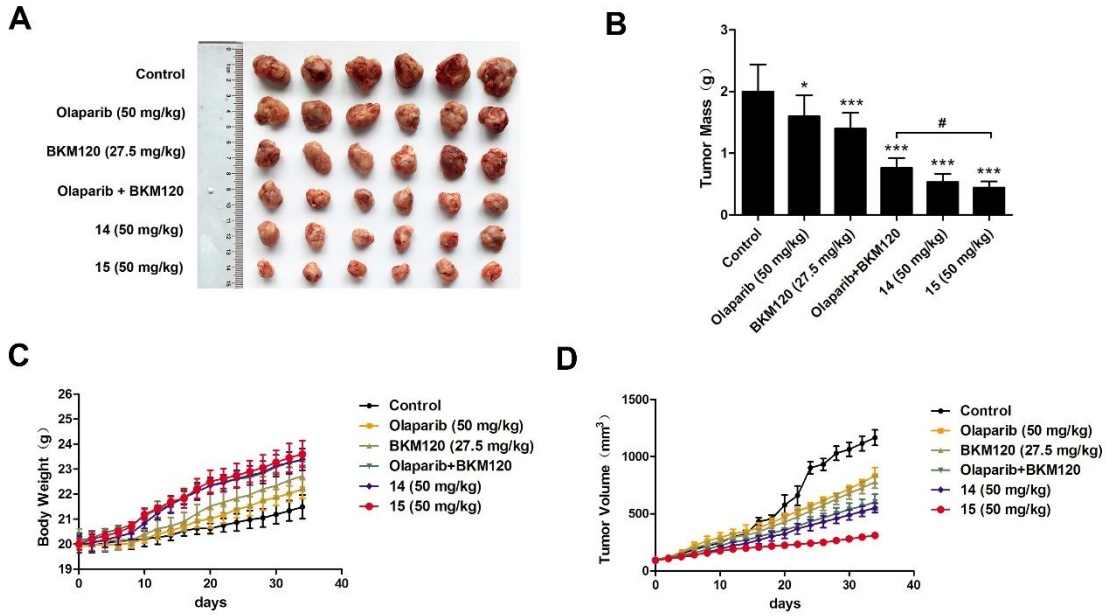

Figure 9. Effects of Olaparib, BKM120, Olaparib (50 mg·kg^{-1}) + BKM120 (27.5 mg·kg^{-1}), compounds **14** and **15** treatment on the tumorigenicity of MDA-MB-468 cells *in vivo*. The combination dose was referred to the literature.[30] (A) The resulting tumors excised from the animals after treatment. (B) The tumor masses for six groups of animals were compared, and each histogram represents the Mean ± SD of 6 mice. *$p < 0.05$ *vs.* control, ***$p < 0.001$; $^{\#}p < 0.05$. (C) The nude mouse body weight was measured every 2 days. (D) The tumor volumes of the nude mice were measured and calculated once every 2 days.

In Vivo Western Blot Analysis.

Since compound **15** displayed more promising antitumor activity *in vivo*, it was submitted to mechanistic study to bolster our conclusion that the prominent antitumor effect of compound **15** is indeed engendered by its PARP/PI3K dual-targeting capability. Western blot analysis of the excised tumor tissue from MDA-MB-468 tumor bearing mice was carried out. In good agreement with the *in vitro* western blot analysis, compound **15** strongly inhibited the expression of pAKT and pS6, while it stimulated the expression of pERK and pETS1 (Figure 10). Moreover, **15** significantly downregulated the expression of BRCA1/2 and increased the level of cleaved PARP. In conclusion,

our medicinal chemistry endeavor led to the discovery of compound **15**, demonstrating that the dual-inhibition of PARP and PI3K with a single chemical entity is feasible.

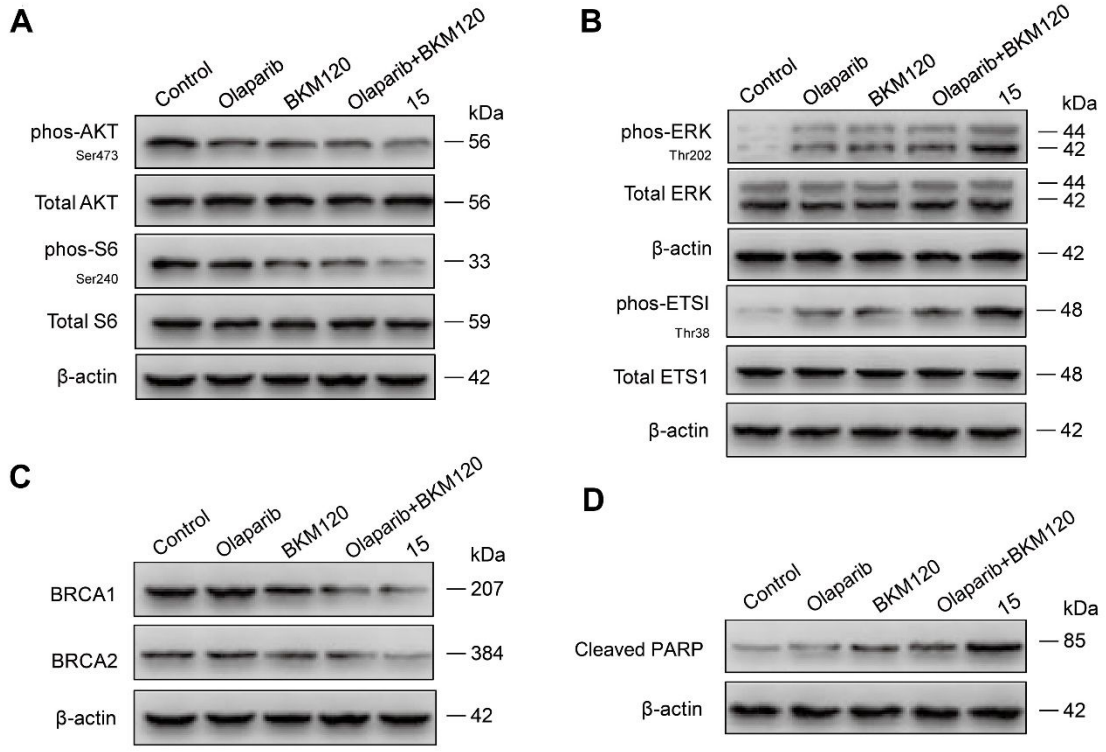

Figure 10. Western blot analysis of the excised tissue from MDA-MB-468 tumor bearing mice after treating with compound **15**. (A) Effects of compound **15** on AKT and S6 phosphorylation levels. (B) Effects of compound **15** on ERK and ETS1 phosphorylation levels. (C) Effects of compound **15** on BRCA1/2 expressions. (D) Effects of compound **15** on cleaved PARP expressions.

Kinase Selectivity Study.

In order to profile compound **15**'s selectivity against PARP and PI3K Isoform, we tested its inhibitory activities against PARP-1/2 and four class I isoforms of PI3K. The results in Table 5 indicate that compound **15** possesses strong inhibitory effect on PARP-1/2 and PI3Kα/δ.

Table 5. PARP and PI3K Isoform Selectivity Profile of Compound 15

Compd	pIC_{50} [a]					
	PARP-1	PARP-2	PI3Kα	PI3Kβ	PI3Kδ	PI3Kγ

15	8.22±0.06	8.44±0.06	8.25±0.09	6.54±0.10	8.13±0.07	6.08±0.05
Olaparib[19]	8.30	9.00				
BKM120[33]			7.28	6.78	6.94	6.58

[a]pIC_{50} values of compound **15** are expressed as the mean ± SD from the dose-response curves of three independent experiments.

To further elucidate its kinase selectivity, compound **15** was tested at a single concentration of 1 μM against 374 kinases in the Reaction Biology Corporation (RBC) kinase panel (see Supporting Information). The results showed that compound **15** displayed weak inhibitory activities against 374 kinases at 1 μM concentration (Figure 11 and Table S1). It can be thus concludes that compound **15** is a highly selective dual PARP/PI3K inhibitor.

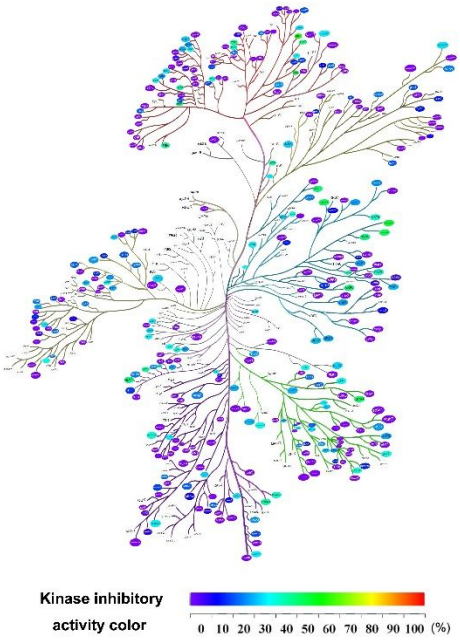

Figure 11. Kinase selectivity profile of compound **15** as shown by an RBC kinase panel screen against 374 kinases assayed at 1 μM in duplicate. Compound selectivity is represented in a dendrogram view of the human kinome phylogenetic tree. The color code for inhibition is indicated.

CHEMISTRY

The synthetic routes of the target compounds are summarized in Schemes 1-3. The synthesis

of compound **1** is depicted in Scheme 1. The starting material 2,4,6-trichloropyrimidine (**20**) was mono-substituted by morpholine to give intermediate **21** which was further substituted by *N*-Boc-piperazine and followed by *N*-deprotection to give intermediate **22**. Condensation of **22** with **23** afforded intermediate **24**. Finally, target compound **1** was obtained by Suzuki coupling of **24** with boric acid ester **25a**.

Scheme 1. Synthetic Route of Compound 1.

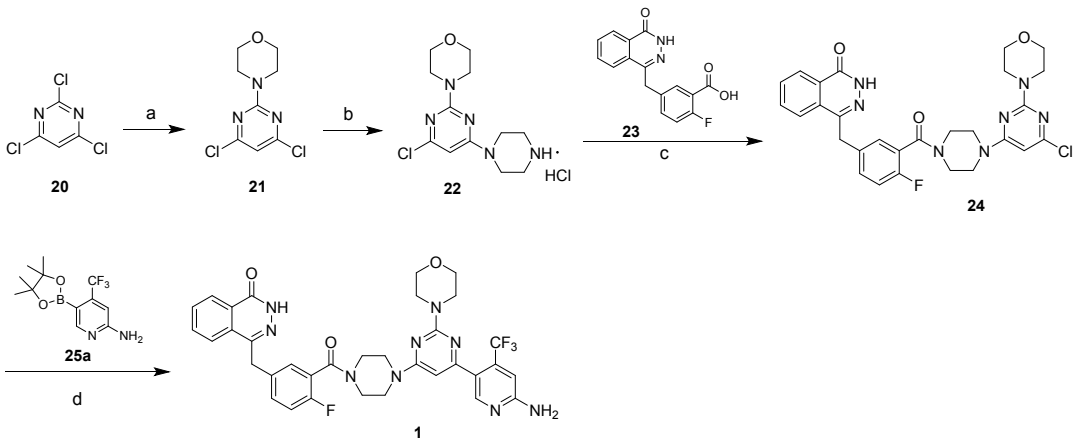

Reagents and conditions: (a) morpholine, DIPEA, DCM, -78 °C, 0.5 h; (b) i) *N*-Boc-piperazine, K_2CO_3, DMF, 25 °C, 5 h; ii) HCl/EtOAc, 25 °C, 2 h; (c) PyBOP, DIPEA, DMF, 25 °C, 6 h; (d) $Pd(PPh_3)_4$, K_2CO_3, dioxane/H_2O, reflux, N_2, 8 h.

Compounds **2-13** were synthesized via a similar route with compound **1** (Scheme 2). The nucleophilic substitution of starting material 2,4,6-trichloro-1,3,5-triazine (**26**) with morpholine produced intermediate **27**, which underwent substitution with *N*-Boc-piperazine and *N*-deprotection giving intermediate **28**. Condensation of **28** with **23** in the presence of PyBOP and DIPEA furnished intermediate **29**. Target compounds **2-13** were finally obtained by Suzuki coupling of **29** with corresponding boric acid esters **25a-l**.

Scheme 2. Synthetic Route of Compounds 2-13.

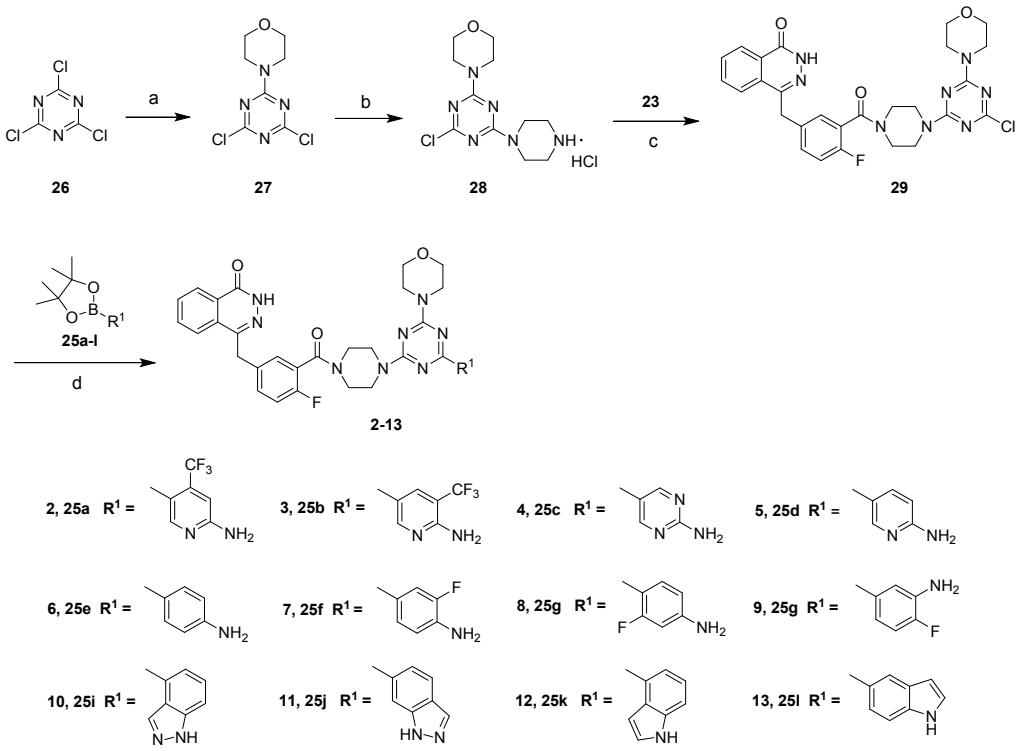

Reagents and conditions: (a) morpholine, DIPEA, DCM, -78 °C, 0.5 h; (b) i) *N*-Boc-piperazine, K_2CO_3, DMF, 25 °C, 5 h; ii) HCl/EtOAc, 25 °C, 2 h; (c) PyBOP, DIPEA, DMF, 25 °C, 6 h; (d) $Pd(PPh_3)_4$, K_2CO_3, dioxane/H_2O, reflux, N_2, 6~8 h.

The synthesis of compounds **14-18** is outlined in Scheme 3. The first step is pinner pyrimidine synthesis, commercially available ethyl 1-benzyl-3-oxopiperidine-4-carboxylate (**30**) was reacted with urea in the presence of NaOMe to produce intermediate **31**. The chlorodehydroxylation of **31** with $POCl_3$ gave intermediate **32** which was further substituted by morpholine and followed by benzyl deprotection to give intermediate **34**. Condensation of **34** with **23** in the presence of PyBOP and DIPEA furnished intermediate **35**. Finally, compounds **14-18** were obtained through Suzuki coupling of **35** with the corresponding boric acid esters.

Scheme 3. Synthetic Route of Compounds 14-18.

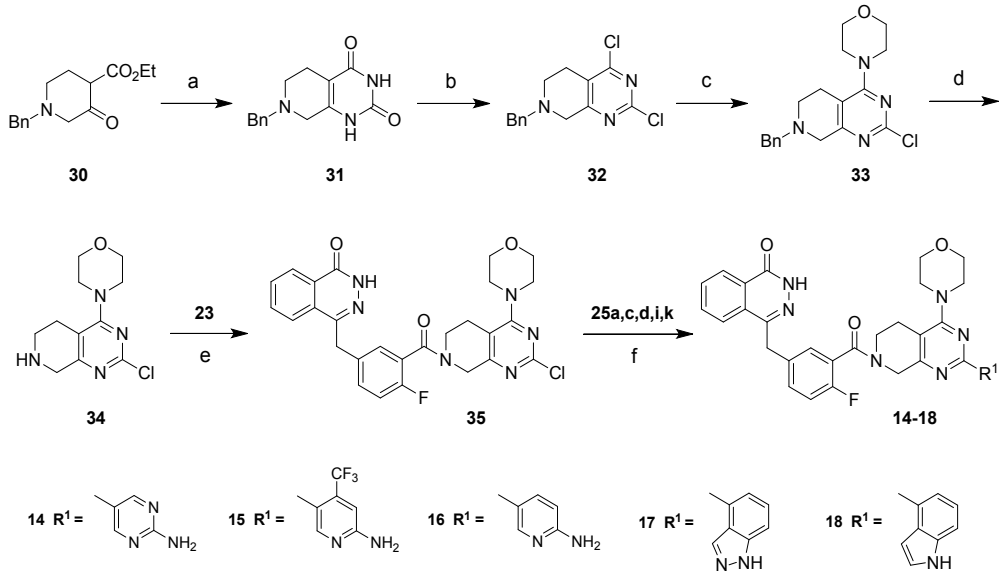

Reaction conditions: (a) urea, NaOMe, MeOH, 0 °C to reflux, N_2, 24 h; (b) $POCl_3$, 0 °C to reflux, N_2, 6 h; (c) morpholine, DIPEA, $(CH_3)_2CHOH/CH_2Cl_2$, 50 °C, 3 h; (d) 1-chloroethyl chloroformate, CH_2Cl_2, 0 to 25 °C, 8 h, MeOH，reflux, 1 h; (e) PyBOP, DIPEA, DMF, 25 °C, 6h; (f) $Pd(PPh_3)_4$, K_2CO_3, dioxane/H_2O, reflux, N_2, 4~6 h.

CONCLUSIONS

PARP inhibitors have clinical effectiveness restricted to a small subgroup of patients with BRCA mutations. Recently, it was reported that PI3K inhibition could promote HR deficiency and sensitize BRCA-proficient tumors to PARP inhibition. Therefore, co-targeting of PARP and PI3K has been recognized as a promising chemotherapeutic strategy to expand the utility of PARP inhibitors. In our efforts to obtain dual PARP/PI3K inhibitors, lead compound **1** was designed by combining the pharmacophores of PARP and PI3K inhibitors. Subsequent structural optimization was conducted, focusing on increasing the inhibitory activities and improving inhibitory balance, and led to the candidate compounds **14** and **15**. They both showed potent and well-balanced inhibitory activities against PARP-1 and PI3Kα with pIC_{50} values greater than 8.22. Compound **15** displayed more potent anti-proliferative activity against a panel of BRCA-proficient cancer cells than Olaparib. Cellular mechanistic studies showed that compounds **14** and **15** strongly inhibited

the growth of MDA-MB-468 cells through suppressing the PI3K signaling pathway, downregulating BRCA1/2 expression and inducing DNA damage and apoptosis. In MDA-MB-468 cell-derived xenograft model, compounds **14** and **15** displayed excellent antitumor efficacy at a dose of 50 $mg \cdot kg^{-1}$, which is considerably more efficacious than the single administration of Olaparib or BKM120 and even their combined administration. In view of the structure together with its encouraging *in vitro* and *in vivo* properties, compound **15** as a first dual PARP/PI3K inhibitor is worthy of further profiling. Our data demonstrate that dual PARP/PI3K inhibitors have good synergistic effect and should be extensively evaluated as a new class of targeted therapy against a wide range of oncologic diseases.

EXPERMENTAL SECTION

General Procedures. Unless otherwise specified, reagents were purchased from commercial suppliers and used without further purification. Melting points were determined by an X-4 digital-display micromelting-point apparatus (Beijing Tech Instrument Company, Ltd., Beijing, China). NMR spectra were recorded on a Bruker AVANCE AV-600 spectrometer (300 MHz and 500 MHz for ^{1}H and 75 MHz for ^{13}C) or a Bruker AVANCE AV-300 spectrometer (300 MHz for ^{1}H and 75 MHz for ^{13}C; Bruker, Billerica, MA). Mass spectra were obtained on an Agilent 1100 LC/MSD mass spectrometer (Agilent, Santa Clara, CA) and Micromass Q-tofmicro MS (Waters, Milford, MA). All reactions were monitored by TLC (Silica gel GF254, Merck, Kenilworth, NJ), and spots were visualized with UV light or iodine. Flash column chromatography on silica gel (200-300 mesh) was used for the routine purification of reaction products. The purities of the biologically evaluated compounds were >95% as determined by HPLC.

General Procedure A for the Synthesis of Compound 1. 2,4,6-trichloropyrimidine **20** (10.00

g, 54.52 mmol) and DIPEA (9.10 mL, 55.06 mmol) were dissolved in dichloromethane (DCM) (100 mL). After cooling to -78 °C, a solution of morpholine (4.75 mL, 54.52 mmol) in DCM (10 mL) was added dropwise. The mixture was stirred at -78 °C for 0.5 h, then the precipitate was filtered and washed with water. The white powder was purified with mixed solvent (n-hexane: ethyl acetate = 50:1, v/v), then filtered and dried in a vacuum desiccator to give intermediate **21** (9.40 g, yield: 74%). m.p.: 122-124 °C. ^{1}H NMR (300 MHz, $CDCl_3$) δ (ppm): 6.56 (1H, s, ArH), 3.83-3.80 (4H, m, $2CH_2O$), 3.76-3.72 (4H, m, $2CH_2N$).

To a solution of compound **21** (2.00 g, 8.54 mmol) in acetone (50 mL) was added *N*-Boc-piperazine (3.98 g, 21.35 mmol) and Et_3N (4.00 mL, 28.86 mmol). The mixture was stirred under reflux for 10 h. After completion, the precipitate was filtered and washed with acetone, then dried under vacuum to give a white solid (2.84 g). The solid was dissolved in ethyl acetate (EtOAc) (15 mL), and an HCl-saturated EtOAc solution was added slowly to pH 2. The mixture was stirred at room temperature until completion of the reaction as evidenced by TLC. The precipitate was filtered, washed with EtOAc and dried under vacuum to give **22** as a white solid (2.36 g, yield: 86%). m.p.: >250 °C. ^{1}H NMR (300 MHz, DMSO-d_6) δ (ppm): 9.53 (1H, s, HCl), 6.92 (1H, s, NH), 6.30 (1H, s, ArH), 3.90 (4H, t, J = 4.8 Hz, $2CH_2O$), 3.67-3.58 (8H, m, $4CH_2N$), 3.12 (4H, s, $2CH_2N$).

To a solution of intermediate **22** (468 mg, 1.46 mmol) in DMF (10 mL) was added compound **23** (436 mg, 1.46 mmol), PyBOP (912 mg, 1.75 mmol) and DIPEA (0.76 mL, 4.38 mmol) dropwise. The mixture was stirred at room temperature for 4 h. After completion, the mixture was poured into water (30 mL) and stirred for 10 min. The precipitate was filtered and washed with water, then dried under vacuum to give intermediate **24** as a yellow solid (650 mg, yield: 79%). m.p.: 108-110 °C. ^{1}H NMR (300 MHz, DMSO-d_6) δ (ppm): 12.57 (1H, s, CONH), 8.25 (1H, d, J = 7.6 Hz, ArH), 7.97-

7.79 (3H, m, ArH), 7.46-7.41 (1H, m, ArH), 7.37-7.34 (1H, m, ArH), 7.22 (1H, t, J = 8.7 Hz, ArH), 6.19 (1H, s, ArH), 4.32 (2H, s, $ArCH_2$), 3.72-3.53 (14H, m, $7CH_2$), 3.24-3.17 (2H, m, CH_2).

4-(3-(4-(6-(6-amino-4-(trifluoromethyl)pyridin-3-yl)-2-morpholinopyrimidin-4-yl)piperazine-1-carbonyl)-4-fluorobenzyl)phthalazin-1(2*H*)-one (1). To a solution of intermediate **24** (0.53 mmol) in dioxane (20 mL) was added boric acid ester **25a** (0.58 mmol), $Pd(PPh_3)_4$ (0.05 mmol) and K_2CO_3 (2.12 mmol) dissolved in water (2 mL). The suspension was heated with stirring under a nitrogen atmosphere at 100 °C for 4-6 h. The reaction was monitored by TLC. After completion of the reaction, the mixture was cooled to room temperature and evaporated under reduced pressure. The residue was partitioned between EtOAc (20 mL) and water (20 mL), and the water phase was extracted two times with the same volume of EtOAc. The combined organic phases were washed with water and brine and evaporated under reduced pressure. The crude product was purified by silica gel column chromatography (DCM/MeOH = 80:1 to 30:1, v/v) to yield title compound **1** as a light yellow solid (148 mg, yield: 41%). m.p.: 142-144 °C. HPLC: 97.7%. ^{1}H NMR (300 MHz, DMSO-d_6+D_2O) δ (ppm): 8.23 (d, J = 7.6 Hz, 1H, ArH), 8.11 (s, 1H, ArH), 7.97-7.89 (m, 1H, ArH), 7.89-7.73 (m, 2H, ArH), 7.44-7.36 (m, 1H, ArH), 7.35-7.27 (m, 1H, ArH), 7.20 (t, J = 9.0 Hz, 1H, ArH), 6.81 (s, 1H, ArH), 6.17 (s, 1H, ArH), 4.30 (s, 2H, $ArNH_2$), 3.80-3.72 (m, 2H, CH_2O), 3.68-3.41 (m, 12H, CH_2O, $5CH_2N$), 3.23-3.08 (m, 2H, CH_2N). ^{13}C-NMR (75 MHz, DMSO-d_6) δ (ppm): 164.2, 162.9, 160.3, 160.0, 159.5, 157.9, 154.7, 152.6, 150.4, 145.2, 140.1, 134.7, 133.6, 131.6, 129.0, 128.7, 127.7, 126.0, 125.4, 123.7, 121.2, 120.4, 116.1, 104.5, 92.0, 65.8, 46.4, 43.8, 36.4, 28.8. HRMS (ESI): m/z $[M+H]^+$. Calcd for $C_{34}H_{32}F_4N_9O_3$: 690.2559; Found: 690.2571. IR (cm^{-1}): 3339.43, 3209.64, 2923.01, 2852.32, 1633.70, 1573.89, 1540.13, 1497.33, 1466.83, 1436.56, 1364.45, 1282.53, 1243.12, 1192.04, 1166.02, 1136.28, 1119.34, 1000.95,

974.15, 806.36, 770.70, 673.73, 483.04.

General Procedure B for the Synthesis of Compounds 2-13. 2,4,6-trichloro-1,3,5-triazine **26** (10.00 g, 54.23 mmol) and DIPEA (9.92 mL, 56.94 mmol) were dissolved in dichloromethane (DCM) (100 mL). After cooling to -78 °C, a solution of morpholine (4.73 mL, 54.23 mmol) in DCM (10 mL) was added dropwise. The mixture was stirred at -78 °C for 0.5 h, then the precipitate was filtered and washed with water. The white powder was dried in a vacuum desiccator to give intermediate **27** (7.18 g, yield: 56%). m.p.: >250 °C. ^{1}H NMR (300 MHz, DMSO-d_6) δ (ppm): 3.80-3.76 (4H, m, CH_2O), 3.69 (4H, t, J = 4.6 Hz, CH_2N).

To a solution of intermediate **27** (7.00 g, 29.78 mmol) in DMF was added *N*-Boc-piperazine (5.55 g, 29.80 mmol) and K_2CO_3 (4.12 g, 29.81 mmol). The mixture was stirred at 25 °C for 5 h. After completion, the mixture was poured into water (300 mL) and stirred for 10 min. The precipitate was filtered and washed with water, then dried under vacuum to give a white solid (10.50 g). Without purification, the white solid was dissolved in ethyl acetate (EtOAc) (50 mL), and then an HCl-saturated EtOAc solution was added slowly to pH 2. The mixture was stirred at room temperature until completion of the reaction as evidenced by TLC. The precipitate was filtered, washed with EtOAc and dried under vacuum to give intermediate **28** as a white solid (7.65 g, yield: 80%). m.p.: >250 °C. ^{1}H NMR (300 MHz, MeOD) δ (ppm): 4.06 (4H, t, J = 5.2 Hz, $2CH_2O$), 3.81-3.77 (4H, m, $2CH_2N$), 3.70-3.67 (4H, m, $2CH_2N$), 3.27 (4H, t, J = 5.4 Hz, $2CH_2N$).

To a solution of intermediate **28** (8.10 g, 25.22 mmol) in DMF (100 mL) was added compound **23** (7.53 g, 25.25 mmol), PyBOP (14.40 g, 27.67 mmol) and DIPEA (12.50 mL, 75.63 mmol) dropwise. The mixture was stirred at room temperature for 6 h. After completion, the mixture was poured into water (300 mL) and stirred for 10 min. The precipitate was filtered and washed with

water, then dried under vacuum. The crude product was purified by silica gel column chromatography (DCM/MeOH = 100:1 to 40:1, v/v) to give intermediate **29** as a light yellow solid (12.50 g, yield: 88%). m.p.: 148-150 °C. ^{1}H-NMR (300 MHz, DMSO-d_6) δ (ppm): 12.57 (1H, s, CONH), 8.27 (1H, d, J = 7.8 Hz, ArH), 7.99-7.81 (3H, m, ArH), 7.48-7.43 (1H, m, ArH), 7.38 (1H, d, J = 6.5 Hz, ArH), 7.25 (1H, t, J = 9.0 Hz, ArH), 4.35 (2H, s, $ArCH_2$), 3.80-3.63 (14H, m, $2CH_2O$, $5CH_2N$), 3.27-3.20 (2H, m, CH_2N).

To a solution of intermediate **29** (0.53 mmol) in dioxane (20 mL) was added boric acid esters **25a-l** (0.58 mmol), $Pd(PPh_3)_4$ (0.05 mmol) and K_2CO_3 (2.12 mmol), which was dissolved in water (2 mL). The suspension was heated with stirring under a nitrogen atmosphere at 100 °C for 4-6 h. The reaction was monitored by TLC. After completion of the reaction, the mixture was cooled to room temperature and evaporated under reduced pressure. The residue was partitioned between EtOAc (20 mL) and water (20 mL), and the water phase was extracted two times with the same volume of EtOAc. The combined organic phases were washed with water and brine and evaporated under reduced pressure. The crude products were purified by silica gel column chromatography (DCM/MeOH = 80:1 to 30:1) to yield title compounds **2-13**.

4-(3-(4-(4-(6-amino-4-(trifluoromethyl)pyridin-3-yl)-6-morpholino-1,3,5-triazin-2-yl)-piperazine-1-carbonyl)-4-fluorobenzyl)phthalazin-1(2*H*)-one (2). Off-white solid, 51% yield, m.p.: 159-161 °C. HPLC: 99.5%. ^{1}H NMR (300 MHz, DMSO-d_6) δ (ppm): 12.61 (1H, s, CONH), 8.61 (1H, s, ArH), 8.27 (1H, d, J = 7.4 Hz, ArH), 7.97 (1H, d, J = 7.4 Hz, ArH), 7.91-7.80 (2H, m, ArH), 7.47-7.43 (1H, m, ArH), 7.39 (1H, dd, J = 6.4, 1.9 Hz, ArH), 7.25 (1H, t, J = 9.0 Hz, ArH), 6.97 (2H, s, NH_2), 6.82 (1H, s, ArH), 4.34 (2H, s, $ArCH_2$), 3.85-3.63 (14H, m, $2CH_2O$, $5CH_2N$), 3.24-3.21 (2H, m, CH_2N). ^{13}C NMR (75 MHz, DMSO-d_6) δ (ppm): 169.5, 164.0, 161.2, 159.3,

158.0, 154.8, 152.6, 144.8, 135.9, 134.8, 133.4, 131.5, 129.1, 127.9, 126.0, 125.4, 124.9, 123.7, 123.5, 121.2, 118.6, 116.1, 115.8, 104.6, 65.9, 46.2, 43.2, 36.5, 28.9. HRMS (ESI): m/z $[M+H]^+$. Calcd for $C_{33}H_{30}F_4N_{10}O_3$: 691.2511; Found: 691.2518. IR (cm^{-1}): 3338.61, 3210.89, 2921.32, 2854.73, 1636.67, 1560.36, 1540.11, 1518.99, 1436.52, 1391.19, 1365.02, 1259.55, 1226.52, 1162.84, 1115.67, 1013.32, 1000.47, 978.32.

4-(3-(4-(4-(6-amino-5-(trifluoromethyl)pyridin-3-yl)-6-morpholino-1,3,5-triazin-2-yl)-piperazine-1-carbonyl)-4-fluorobenzyl)phthalazin-1(2*H*)-one (3). Light yellow solid, 55% yield, m.p.: 244-246 °C. ^{1}H NMR (300 MHz, DMSO-d_6) δ (ppm): 12.62 (1H, s, CONH), 9.12 (1H, s, ArH), 8.48 (1H, s, ArH), 8.26 (1H, d, J = 7.3 Hz, ArH), 7.99-7.80 (3H, m, ArH), 7.49-7.35 (2H, m, ArH), 7.26 (1H, t, J = 8.9 Hz, ArH), 7.14 (1H, s, 1/2NH_2), 6.42 (1H, s, 1/2NH_2) 4.35 (2H, s, $ArCH_2$), 3.94-3.51(14H, m, 2CH_2O, 5CH_2N), 3.22 (2H, m, CH_2N). ^{13}C NMR (75 MHz, DMSO-d_6) δ (ppm): 167.4, 164.2, 164.0, 161.0, 159.3, 158.0, 157.3, 154.8, 153.2, 151.3, 144.8, 138.8, 134.8, 133.4, 131.6, 129.1, 128.9, 127.9, 126.0, 125.5, 123.8, 119.8, 116.1, 115.8, 66.0, 45.8, 43.1, 36.4, 25.8. HRMS (ESI): m/z $[M+H]^+$. Calcd for $C_{33}H_{30}F_4N_{10}O_3$: 691.2511; Found: 691.2517. IR (cm^{-1}): 3518.20, 3178.15, 2897.79, 2858.70, 1680.81, 1645.80, 1583.50, 1544.76, 1522.47, 1497.79, 1441.61, 1396.66, 1363.34, 1308.66, 1253.94, 1225.60, 1148.85, 1114.30, 1003.38, 983.10, 814.27, 681.51.

4-(3-(4-(4-(2-aminopyrimidin-5-yl)-6-morpholino-1,3,5-triazin-2-yl)piperazine-1-carbonyl)-4-fluorobenzyl)phthalazin-1(2*H*)-one (4). Light yellow solid, 58% yield, m.p.: 182-183 °C. HPLC: 98.4%. ^{1}H NMR (300 MHz, DMSO-d_6) δ (ppm): 12.61 (1H, s, CONH), 9.06 (2H, s, ArH), 8.26 (1H, d, J = 6.8 Hz, ArH), 7.99-7.81 (3H, m, ArH), 7.49-7.43 (1H, m, ArH), 7.38 (1H, d, J = 6.6, 1.9 Hz, ArH), 7.30 (2H, s, NH_2), 7.25-7.22 (1H, m, ArH), 4.34 (2H, s, $ArCH_2$), 3.94-3.57

(14H, m, $7CH_2$), 3.26-3.19 (2H, m, CH_2). ^{13}C NMR (75 MHz, DMSO-d_6) δ (ppm): 167.3, 164.8, 164.2, 164.0, 159.3, 158.6, 158.0, 154.8, 144.8, 134.8, 133.4, 131.5, 129.1, 128.9, 127.9, 126.0, 125.4, 123.8, 118.5, 116.1, 115.8, 66.0, 46.4, 43.2, 41.2, 36.4. HRMS (ESI): m/z $[M+H]^+$. Calcd for $C_{31}H_{30}FN_{11}O_3$: 624.2590; Found: 624.2595. IR (cm^{-1}): 3400.94, 3172.76, 3068.06, 2857.65, 1635.53, 1567.75, 1521.30, 1441.00, 1411.71, 1352.79, 1263.93, 1225.51, 1198.73, 1113.79, 1000.91, 978.00, 811.87, 785.84, 491.72.

4-(3-(4-(4-(6-aminopyridin-3-yl)-6-morpholino-1,3,5-triazin-2-yl)piperazine-1-carbonyl)-4-fluorobenzyl)phthalazin-1(2*H*)-one (5). Light yellow solid, 49% yield, m.p.: 180-182 °C. ^1H NMR (300 MHz, DMSO-d_6) δ (ppm): 12.61 (1H, s, CONH), 8.89 (1H, s, ArH), 8.26-8.19 (2H, m, ArH), 7.97-7.79 (3H, m, ArH), 7.46-7.37 (2H, m, ArH), 7.24 (1H, t, J = 8.7 Hz, ArH), 6.57 (2H, s, $ArNH_2$), 6.45 (1H, d, J = 8.4 Hz, ArH), 4.33 (2H, s, $ArCH_2$), 3.93-3.64 (14H, m, $2CH_2O$, $5CH_2N$), 3.27-3.18 (2H, m, CH_2N). ^{13}C NMR (75 MHz, DMSO-d_6) δ (ppm): 168.6, 164.3, 164.0, 161.9, 159.3, 154.8, 149.7, 144.8, 136.7, 134.8, 133.4, 131.5, 129.1, 127.9, 126.0, 125.4, 123.8, 123.5, 120.1, 118.2, 116.1, 115.8, 106.9, 66.0, 46.3, 43.2, 41.2, 36.4. HRMS (ESI): m/z $[M+H]^+$. Calcd for $C_{32}H_{32}FN_{10}O_3$: 623.2637; Found: 623.2647. IR (cm^{-1}): 3346.35, 3212.54, 2898.01, 2855.28, 1635.62, 1572.82, 1536.84, 1520.76, 1437.02, 1387.93, 1363.78, 1259.18, 1227.87, 1112.93, 1000.40, 977.48, 812.87, 771.39.

4-(3-(4-(4-(4-aminophenyl)-6-morpholino-1,3,5-triazin-2-yl)piperazine-1-carbonyl)-4-fluorobenzyl)phthalazin-1(2*H*)-one (6). Off-white solid, 33% yield, m.p.: 168-170 °C. ^1H NMR (300 MHz, $CDCl_3$) δ (ppm): 10.42 (1H, s, CONH), 8.47 (1H, d, J = 8.0 Hz, ArH), 8.20 (2H, d, J = 8.0 Hz, ArH), 7.80-7.73 (3H, m, ArH), 7.39-7.27 (2H, m, ArH), 7.05 (1H, t, J = 8.6 Hz, ArH), 6.71 (2H, d, J = 7.7 Hz, ArH), 4.30 (2H, s, $ArCH_2$), 4.14-3.77 (14H, m, $2CH_2O$, $5CH_2N$), 3.46-3.36 (2H,

m, CH_2N). ^{13}C NMR (75 MHz, DMSO-d_6) δ (ppm): 169.5, 164.5, 163.8, 159.3, 158.0, 154.8, 152.3, 144.8, 134.8, 133.4, 131.5, 129.8, 129.1, 128.9, 127.9, 126.1, 125.5, 123.8, 123.3, 116.1, 115.8, 112.7, 66.0, 46.3, 43.2, 41.3, 36.4. HRMS (ESI): m/z $[M+H]^+$. Calcd for $C_{33}H_{32}FN_9O_3$: 622.2685; Found: 622.2697. IR (cm^{-1}): 3354.38, 3227.25, 2855.64, 1646.35, 1581.07, 1535.62, 1520.93, 1438.37, 1390.32, 1363.98, 1259.48, 1227.42, 1168.19, 1114.56, 1001.14, 977.86, 810.79, 771.91.

4-(3-(4-(4-(4-amino-3-fluorophenyl)-6-morpholino-1,3,5-triazin-2-yl)piperazine-1-carbonyl)-4-fluorobenzyl)phthalazin-1(2*H*)-one (7). Light yellow solid, 59% yield, m.p.: 138-140 °C. HPLC: 99.1%. ^1H NMR (300 MHz, $CDCl_3$) δ (ppm): 10.23 (1H, s, CONH), 8.49-8.46 (1H, m, ArH), 8.04-7.99 (2H, m, ArH), 7.83-7.72 (3H, m, ArH), 7.39-7.31 (2H, m, ArH), 7.06 (1H, t, J = 8.7 Hz, ArH), 6.79 (1H, t, J = 8.0 Hz, ArH), 4.30 (2H, s, $ArCH_2$), 4.20-3.77 (14H, m, $2CH_2NO$, $5CH_2N$), 3.46-3.37 (2H, m, CH_2N). ^{13}C NMR (75 MHz, DMSO-d_6) δ (ppm): 168.7, 164.4, 164.0, 159.4, 158.0, 154.8, 151.3, 148.2, 144.8, 140.2, 134.8, 133.4, 131.7, 131.5, 129.1, 128.6, 127.9, 126.0, 125.4, 124.1, 123.5, 115.8, 114.8, 114.3, 66.0, 46.4, 43.2, 41.3, 36.4. HRMS (ESI): m/z $[M+H]^+$. Calcd for $C_{33}H_{31}F_2N_9O_3$: 640.2591; Found: 640.2590. IR (cm^{-1}): 3350.16, 3209.97, 2897.72, 2855.52, 1670.18, 1635.86, 1541.59, 1480.38, 1437.27, 1383.95, 1364.01, 1303.30, 1258.28, 1227.56, 1148.32, 1113.70, 1001.71, 982.63, 909.77, 808.56, 790.79, 771.09, 740.46.

4-(3-(4-(4-(4-amino-2-fluorophenyl)-6-morpholino-1,3,5-triazin-2-yl)piperazine-1-carbonyl)-4-fluorobenzyl)phthalazin-1(2*H*)-one (8). Off-white solid, 49% yield, m.p.: 109-111 °C. ^1H NMR (300 MHz, $CDCl_3$) δ (ppm): 10.28 (1H, s, CONH), 8.49 (1H, s, ArH), 7.97 (1H, s, ArH), 7.87-7.23 (3H, m, ArH), 7.40-7.32 (2H, m, ArH), 7.07 (1H, t, J = 8.4 Hz, ArH), 6.50-6.38 (2H, m, ArH), 4.31 (2H, s, $ArCH_2$), 4.11-3.68 (12H, m, $2CH_2O$, $4CH_2N$), 3.51-3.20 (4H, m, $2CH_2N$). ^{13}C NMR (75 MHz, DMSO-d_6) δ (ppm): 168.5, 164.9, 164.3, 164.0, 161.5, 159.3, 154.8, 153.7,

144.8, 134.8, 133.4, 132.4, 131.5, 129.1, 128.9, 127.9, 126.0, 125.5, 123.8, 116.1, 115.8, 111.2, 109.2, 100.0, 66.0, 45.9, 43.2, 36.4, 24.9. HRMS (ESI): m/z $[M+H]^+$. Calcd for $C_{33}H_{31}F_2N_9O_3$: 640.2591; Found: 640.2589. IR (cm^{-1}): 3353.59, 3231.40, 2856.78, 2360.98, 1634.99, 1577.85, 1535.76, 1475.57, 1437.51, 1389.37, 1364.58, 1269.74, 1226.83, 1172.82, 1157.33, 1113.12, 1015.05, 1000.81, 978.24, 952.05, 844.92, 809.41, 789.51, 771.68, 590.01, 559.00, 488.77.

4-(3-(4-(4-(3-amino-4-fluorophenyl)-6-morpholino-1,3,5-triazin-2-yl)piperazine-1-carbonyl)-4-fluorobenzyl)phthalazin-1(2*H*)-one (9). Off-white solid, 46% yield, m.p.: 133-135 °C. ^{1}H NMR (300 MHz, $CDCl_3$) δ (ppm): 10.70 (1H, s, CONH), 8.48 (1H, d, J = 7.9 Hz, ArH), 7.87 (1H, d, J = 8.5 Hz, ArH), 7.80-7.73 (3H, m, ArH), 7.40-7.32 (3H, m, ArH), 7.10-7.00 (2H, m, ArH), 4.31 (2H, s, $ArCH_2$), 4.06-3.67 (14H, m, $2CH_2O$, $5CH_2N$), 3.44-3.38 (2H, m, CH_2 N). ^{13}C NMR (75 MHz, DMSO-d_6) δ (ppm): 169.2, 164.5, 164.0, 159.4, 158.0, 154.8, 154.4, 151.2, 144.9, 136.0, 134.8, 133.5, 133.0, 131.5, 129.1, 128.7, 127.9, 126.1, 125.4, 116.5, 116.2, 115.8, 114.7, 114.4, 66.0, 46.3, 43.2, 41.2, 36.4. HRMS (ESI): m/z $[M+H]^+$. Calcd for $C_{33}H_{31}F_2N_9O_3$: 640.2591; Found: 640.2597. IR (cm^{-1}): 3376.39, 2895.40, 2857.80, 2351.02, 1657.85, 1626.49, 1557.36, 1474.24, 1439.01, 1388.73, 1330.16, 1224.77, 1202.17, 1172.05, 1114.62, 1020.31, 1003.45, 985.39, 800.21, 770.29, 741.28, 614.93, 541.60, 490.12.

4-(3-(4-(4-(1H-indazol-4-yl)-6-morpholino-1,3,5-triazin-2-yl)piperazine-1-carbon-yl)-4-fluorobenzyl)phthalazin-1(2*H*)-one (10). White solid, 39% yield, m.p.: 178-180 °C. ^{1}H NMR (300 MHz, $CDCl_3$) δ (ppm): 11.19 (1H, s, NH), 10.75 (1H, s, CONH), 8.85 (1H, s, ArH), 8.48 (1H, d, J = 6.5 Hz, ArH), 8.28 (1H, d, J = 6.6 Hz, ArH), 7.78-7.72 (3H, m, ArH), 7.67 (1H, d, J = 8.4 Hz, ArH), 7.49-7.32 (3H, m, ArH), 7.05 (1H, q, J = 9.1 Hz, ArH), 4.31 (2H, s, $ArCH_2$), 4.16-3.71 (14H, m, $2CH_2O$, $5CH_2N$), 3.45-3.31 (2H, m, CH_2N). ^{13}C NMR (75 MHz, DMSO-d_6) δ (ppm): 173.5,

170.1, 164.6, 164.0, 159.4, 151.1, 144.8, 140.6, 134.8, 134.6, 133.4, 131.5, 129.6, 129.1, 128.9, 127.9, 126.0, 125.5, 123.5, 122.1, 120.8, 116.1, 115.8, 114.5, 1137, 66.0, 45.8, 43.2, 36.5, 25.9. HRMS (ESI): m/z $[M+H]^+$. Calcd for $C_{34}H_{31}FN_{10}O_3$: 647.2637; Found: 647.2629. IR (cm^{-1}): 3217.77, 2896.84, 2856.59, 1653.16, 1545.69, 1517.80, 1483.59, 1436.78, 1354.26, 1272.14, 1258.09, 1226.80, 1170.98, 1113.19, 1068.68, 999.79, 974.46, 927.76, 853.90, 795.20, 769.31, 747.06, 543.51, 486.83.

4-(3-(4-(4-(1H-indazol-6-yl)-6-morpholino-1,3,5-triazin-2-yl)piperazine-1-carbonyl)-4-fluorobenzyl)phthalazin-1(2*H*)-one (11). Light yellow solid, 43% yield, m.p.: 145-147 °C. ^{1}H NMR (300 MHz, $CDCl_3$) δ (ppm): 10.71 (1H, s, CONH), 8.62-8.48 (2H, m, ArH), 8.19-8.12 (1H, m, ArH), 7.89-7.68 (4H, m, ArH), 7.56-7.33 (3H, m, ArH), 7.05 (1H, J = 9.5 Hz, ArH), 4.28 (2H, s, $ArCH_2$), 4.01-3.72 (12H, m, $2CH_2O$, $4CH_2N$), 3.43-3.19 (4H, m, $2CH_2N$). ^{13}C NMR (75 MHz, DMSO-d_6) δ (ppm): 169.8, 164.6, 164.0, 159.3, 158.0, 154.7, 144.8, 139.8, 134.8, 134.5, 133.4, 131.7, 131.5, 129.0, 127.9, 126.0, 125.4, 124.8, 123.7, 123.5, 120.0, 116.0, 115.8, 110.2, 100.3, 66.0, 45.8, 43.2, 36.4, 26.0. HRMS (ESI): m/z $[M+H]^+$. Calcd for $C_{34}H_{31}FN_{10}O_3$: 647.2637; Found: 647.2646. IR (cm^{-1}): 3446.07, 2856.25, 2360.41, 2341.71, 1653.52, 1581.31, 1543.43, 1520.01, 1490.55, 1436.72, 1360.20, 1304.99, 1254.23, 1226.07, 1171.75, 1112.74, 1000.25, 980.05, 940.13, 846.74, 805.58, 771.99.

4-(3-(4-(4-(1H-indol-4-yl)-6-morpholino-1,3,5-triazin-2-yl)piperazine-1-carbonyl)-4-fluorobenzyl)phthalazin-1(2*H*)-one (12). Light yellow solid, 47% yield, m.p.: 166-168 °C. HPLC: 99.1%. ^{1}H NMR (300 MHz, $CDCl_3$) δ (ppm): 10.87 (1H, s, CONH), 8.56 (1H, s, ArH), 8.48 (1H, d, J = 7.3 Hz, ArH), 8.22 (1H, s, ArH), 7.82-7.72 (3H, m, ArH), 7.52 (1H, d, J = 7.5 Hz, ArH), 7.42-7.32 (4H, m, ArH), 7.07 (1H, t, J = 8.7 Hz, ArH), 4.31 (2H, s, $ArCH_2$), 4.16-3.82 (14H, m, $2CH_2O$,

5CH_2N), 3.50-3.39 (2H, m, CH_2N). ^{13}C NMR (75 MHz, DMSO-d_6) δ (ppm): 171.5, 164.7, 164.0, 159.4, 158.0, 154.8, 144.8, 137.0, 134.8, 133.4, 131.5, 129.1, 128.9, 128.1, 127.9, 126.5, 126.1, 125.4, 123.8, 123.5, 121.1, 120.2, 116.1, 115.8, 114.9, 103.2, 66.0, 46.3, 43.4, 41.3, 36.5. HRMS (ESI): m/z $[M+H]^+$. Calcd for $C_{35}H_{32}FN_9O_3$: 646.2685; Found: 646.2677. IR (cm^{-1}): 3268.85, 2896.46, 2853.54, 1658.76, 1541.35, 1519.88, 1495.99, 1436.10, 1394.89, 1363.03, 1334.69, 1271.89, 1258.35, 1225.68, 1169.46, 1111.35, 998.04, 824.28, 798.53, 762.84.

4-(3-(4-(4-(1H-indol-5-yl)-6-morpholino-1,3,5-triazin-2-yl)piperazine-1-carbonyl)-4-fluorobenzyl)phthalazin-1(2*H*)-one (13). Light yellow solid, 39% yield, m.p.: 123-125 °C. ^{1}H NMR (300 MHz, $CDCl_3$) δ (ppm): 10.30 (1H, s, CONH), 8.73 (1H, s, NH), 8.48-8.40 (2H, m, ArH), 8.27-8.23 (1H, m, ArH), 7.82-7.72 (3H, m, ArH), 7.40-7.30 (3H, m, ArH), 7.23 (1H, s, ArH), 7.06 (1H, t, J = 8.9 Hz, ArH), 6.63 (1H, s, ArH), 4.29 (2H, s, ArCH_2), 4.19-3.72 (14H, m, 2CH_2O, 5CH_2N), 3.49-3.40 (2H, m, CH_2N). ^{13}C NMR (75 MHz, DMSO-d_6) δ (ppm): 170.6, 164.6, 164.0, 159.4, 158.0, 154.8, 144.9, 138.1, 134.8, 133.5, 131.5, 129.1, 128.6, 127.9, 127.4, 126.4, 126.1, 125.5, 123.7, 123.5, 121.5, 121.1, 116.1, 115.8, 110.8, 102.3, 66.0, 61.9, 46.3, 43.3, 36.4. HRMS (ESI): m/z $[M+H]^+$. Calcd for $C_{35}H_{32}FN_9O_3$: 646.2685; Found: 646.2691. IR (cm^{-1}): 3410.99, 2896.94, 2854.69, 1743.76, 1655.33, 1543.04, 1520.93, 1486.14, 1436.61, 1385.05, 1364.15, 1272.03, 1257.68, 1227.36, 1171.11, 1112.66, 1068.68, 1013.99, 1000.56, 979.44, 849.51, 806.55, 771.10, 741.19, 542.63, 479.77.

General Procedure C for the Synthesis of Compound 14-18.

To a solution of compound **30** (40.00 g, 134.33 mmol) and urea (17.09 g, 282.01 mmol) in anhydrous methanol (MeOH, 250 mL) was added sodium methoxide (228.00 mL, 1 mol/L) at 0 °C. The mixture was stirred at reflux temperature for 8 h under a nitrogen atmosphere. After completion,

the mixture was cooled to room temperature and stirred at 0 °C for 1 h. The precipitate was filtered and washed with MeOH (50 mL), then dissolved in water (400 mL) and adjust the pH to 7 with 1 mol/L HCl. The precipitate was filtered and washed with water, then dried under vacuum to give compound **31** as white solid (27.68 g, yield: 80%), which was used for further reactions without purification.

Compound **31** (27.68 g, 107.58 mmol) was slowly added into $POCl_3$ (200 mL) at 0 °C. The mixture was heated to reflux for 6~8 h under a nitrogen atmosphere. After completion, the mixture was cooled to room temperature and evaporated under reduced pressure. The residue was poured into ice-water (400 mL) and the pH was adjusted to 8~9. The precipitate was filtered and washed with water, then dried under vacuum to give compound **32** as off-white solid (29.0 g, yield: 92%). m.p.: >250 °C. ^{1}H NMR (300 MHz, $CDCl_3$) δ (ppm): 7.34-7.29 (5H, m, ArH), 3.75 (2H, s, $BnCH_2$), 3.67 (2H, s, $ArCH_2N$), 2.85 (4H, s, NCH_2CH_2).

To a solution of compound **32** (29.0 g, 98.58 mmol) in isopropanol (200 mL) was added morpholine (10.31 g, 118.30 mmol) and DIPEA (32.59 mL, 197.16 mmol). The mixture was stirred at 50 °C for 5 h. After completion, the mixture was cooled to room temperature and stirred at 0 °C for 0.5 h. The precipitate was filtered, washed with isopropanol and dried under vacuum to give compound **33** as white solid (30.42 g, yield: 90%). m.p.: 154-156 °C. ^{1}H NMR (300 MHz, DMSO-d_6) δ (ppm): 7.34-7.23 (5H, m, ArH), 3.66-3.62 (6H, m, $2CH_2O$, $PhCH_2$), 3.47-3.44 (6H, m, $ArCH_2CH_2N$, $ArCH_2N$), 2.65-2.54 (4H, m, $2CH_2N$).

To a solution of compound **33** (21.10 g, 61.19 mmol) in DCM (200 mL) was added 1-chloroethyl carbonochloridate (26.41 mL, 244.76 mmol) at 0 °C. The mixture was stirred at 25 °C for 10 h. After completion, the solvent was evaporated under reduced pressure. The residue was

dissolved in MeOH (200 mL) and heated to reflux for 1 h, then the solvent was evaporated under reduced pressure. The residue was dissolved in water (200 mL), and after the pH was adjusted to 8~9 with 1mol/L NaOH, the water phase was extracted with DCM (150 mL×3). The combined organic phase was washed with water and brine, dried over Na_2SO_4 overnight, and the solvent was evaporated under vacuum. The crude product was purified by silica gel column chromatography (DCM/MeOH = 80:1 to 20:1, v/v) to yield compound **34** as yellow solid (10.5 g, yield: 67%). ^{1}H NMR (300 MHz, DMSO-d_6) δ (ppm): 3.75-3.64 (6H, m, $ArCH_2N$, $2CH_2O$), 3.44-3.41 (4H, m, $ArCH_2CH_2N$), 2.79 (2H, t, J = 5.3 Hz, CH_2N), 2.66 (1H, s, NH), 2.50-2.48 (2H, m, CH_2N).

To a solution of compound **34** (9.60 g, 37.69 mmol) in DMF (100 mL) was added compound **23** (11.24 g, 37.68 mmol), PyBOP (11.24 g, 37.68 mmol) and DIPEA (24.92 mL, 150.79 mmol) dropwise. The mixture was stirred at room temperature for 4 h. After completion, the mixture was poured into water (300 mL) and stirred for 10 min. The precipitate was filtered and washed with water, then dried under vacuum. The crude product was purified by silica gel column chromatography (DCM/MeOH = 100:1 to 20:1, v/v) to yield compound **35** as off-white solid (12.06 g, 60%). m.p.: 174-177 ^{o}C. ^{1}H NMR (300 MHz, DMSO-d_6) δ (ppm): 12.61 (1H, s, CONH), 8.29-8.25 (1H, m, ArH), 7.98 (1H, d, J = 7.7 Hz, ArH), 7.92-7.80 (2H, m, ArH), 7.52-7.40 (2H, m, ArH), 7.32-7.24 (1H, m, ArH), 4.63 (1H, s, 1/2$ArCH_2N$), 4.36 (2H, s, $ArCH_2$), 4.29 (1H, s, 1/2$ArCH_2N$), 3.85-3.61 (5H, m, $2CH_2$, 1/2CH_2), 3.54-3.42 (4H, m, $2CH_2$), 3.29-3.13 (1H, m, 1/2CH_2), 2.74-2.57 (2H, m, NCH_2CH_2).

To a solution of compound **35** (0.53 mmol) in dioxane (20 mL) was added the corresponding boric acid esters (0.58 mmol), $Pd(PPh_3)_4$ (0.05 mmol) and K_2CO_3 (2.12 mmol) which was dissolved in water (2 mL). The suspension was heated with stirring under a nitrogen atmosphere at 100 °C for

4-6 h. The reaction was checked by TLC. After completion of the reaction, the mixture was cooled to room temperature and evaporated under reduced pressure. The residue was partitioned between EtOAc (20 mL) and water (20 mL), and the water phase was extracted two times with the same volume of EtOAc. The combined organic phases were washed with water and brine and evaporated under reduced pressure. The crude product was purified by silica gel column chromatography (DCM/MeOH = 100:1 to 20:1, v/v) to yield the title compounds **14-18**.

4-(3-(2-(2-aminopyrimidin-5-yl)-4-morpholino-5,6,7,8-tetrahydropyrido[3,4-d]pyrimidine-7-carbonyl)-4-fluorobenzyl)phthalazin-1(2*H*)-one (14). Light yellow solid, 58% yield, m.p.: 159-160 °C. HPLC: 99.1%. ^{1}H NMR (300 MHz, DMSO-d_6) δ (ppm): 12.73 (1H, s, CONH), , 9.16 (1H, s, ArH), 9.07 (1H, s, ArH), 8.37 (1H, t, J = 6.8 Hz, ArH), 8.11-7.88 (3H, m, ArH), 7.63-7.54 (2H, m, ArH), 7.40 (1H, t, J = 8.7 Hz, ArH), 7.30 (2H, s, NH_2), 4.81 (1H, s, 1/2ArCH_2N), 4.47 (2H, s, ArCH_2), 4.45 (1H, s, 1/2ArCH_2N), 3.95-3.55 (10H, m, 5CH_2), 2.85-2.71 (2H, m, NCH$_2$CH$_2$). ^{13}C-NMR (75 MHz, DMSO-d_6) δ (ppm): 164.1, 163.7, 162.7, 160.3, 159.9, 159.3, 157.8, 154.9, 144.9, 134.9, 133.4, 132.0, 131.5, 129.1, 127.9, 126.0, 125.4, 123.7, 119.5, 117.8, 115.9, 112.4, 66.0, 50.5, 47.7, 46.4, 36.4, 26.1. HRMS (ESI): m/z $[M+H]^+$. Calcd for $C_{31}H_{29}FN_9O_3$: 594.2372; Found: 594.2371. IR (cm^{-1}): 3439.10, 3056.05, 2855.46, 2359.88, 1776.06, 1612.09, 1544.18, 1496.85, 1442.30, 1362.38, 1265.64, 1229.74, 1111.78, 1020.77, 771.11.

4-(3-(2-(6-amino-4-(trifluoromethyl)pyridin-3-yl)-4-morpholino-5,6,7,8-tetrahydropyrido-[3,4-d]pyrimidine-7-carbonyl)-4-fluorobenzyl)phthalazin-1(2*H*)-one (15). Light yellow solid, 55% yield, m.p.: 158-160 °C. HPLC: 97.6%. ^{1}H-NMR (300 MHz, DMSO-d_6) δ (ppm): 12.56 (1H, s, CONH), 8.51-8.42 (1H, m, ArH), 8.25 (1H, t, J = 7.3 Hz, ArH), 7.98-7.75 (3H, m, ArH), 7.50-7.43 (2H, m, ArH), 7.30-7.22 (1H, m, ArH), 6.82 (1H, s, ArH), 6.80 (2H, s, NH_2),

4.68 (1H, s, 1/2ArCH$_2$N), 4.35 (2H, s, ArCH$_2$), 4.32 (1H, s, 1/2ArCH$_2$N), 3.84-3.39 (10H, m, 5CH$_2$), 2.76-2.60 (2H, m, NCH$_2$CH$_2$). ^{13}C-NMR (75 MHz, DMSO-d_6) δ (ppm): 164.4, 164.0, 163.6, 160.5, 159.8, 159.4, 158.2, 155.0, 152.4, 144.8, 135.6, 134.9, 133.4, 132.0, 131.5, 129.1, 127.9, 126.0, 125.4, 123.5, 121.3, 119.7, 116.1, 112.6, 104.4, 66.0, 47.7, 46.3, 43.6, 36.5, 26.0. HRMS (ESI): m/z $[M+H]^+$. Calcd for $C_{33}H_{29}F_4N_8O_3$: 661.2293; Found: 661.2298. IR (cm^{-1}): 3338.35, 3209.36, 2853.42, 1635.92, 1566.26, 1496.19, 1436.91, 1403.71, 1363.71, 1266.13, 1228.77, 1145.56, 1114.27, 1044.47, 1015.82, 941.47, 799.05, 772.14, 678.60.

4-(3-(2-(6-aminopyridin-3-yl)-4-morpholino-5,6,7,8-tetrahydropyrido[3,4-d]pyrimidine-7-carbonyl)-4-fluorobenzyl)phthalazin-1(2*H*)-one (16). Light yellow solid, 66% yield, m.p.: 206-207 °C. HPLC: 98.1%. ^{1}H NMR (300 MHz, DMSO-d_6) δ (ppm): 12.61 (1H, s, CONH), 8.89-8.80 (1H, m, ArH), 8.28-8.12 (2H, m, ArH), 8.00-7.78 (3H, m, ArH), 7.51-7.45 (2H, m, ArH), 7.29 (1H, t, J = 9.1 Hz, ArH), 6.51-6.47 (1H, m, ArH), 6.44 (2H, s, NH$_2$), 4.69 (1H, s, 1/2ArCH$_2$N), 4.36 (2H, s, ArCH$_2$), 4.33 (1H, s, 1/2ArCH$_2$N), 3.88-3.47 (10H, m, 5CH$_2$), 2.73-2.58 (2H, m, NCH$_2$CH$_2$). ^{13}C-NMR (75 MHz, DMSO-d_6) δ (ppm): 164.4, 163.8, 161.0, 160.2, 159.8, 159.4, 155.0, 148.6, 144.9, 136.2, 134.9, 133.4, 132.0, 131.5, 129.1, 127.9, 126.0, 125.4, 123.8, 121.3, 116.1, 115.8, 111.9, 107.2, 66.0, 47.8, 46.5, 43.7, 36.5, 26.0. HRMS (ESI): m/z $[M+H]^+$. Calcd for $C_{32}H_{30}FN_8O_3$: 593.2419; Found: 593.2418. IR (cm^{-1}): 3619.75, 3427.21, 2843.66, 2360.67, 2342.16, 1672.48, 1637.96, 1570.73, 1559.89, 1541.40, 1438.73, 1404.19, 1263.35, 1225.96, 1113.45, 1015.84, 936.28, 791.75, 430.43.

4-(3-(2-(1H-indazol-4-yl)-4-morpholino-5,6,7,8-tetrahydropyrido[3,4-d]pyramidine-7-carbonyl)-4-fluorobenzyl)phthalazin-1(2*H*)-one (17). Light yellow solid, 40% yield, m.p.: 198-200 °C. HPLC: 99.3%. ^{1}H NMR (300 MHz, DMSO-d_6) δ (ppm): 13.24 (1H, s, NH), 12.60 (1H, s,

CONH), 8.82-8.70 (1H, m, ArH), 8.28-8.07 (2H, m, ArH), 7.97 (t, *J* = 7.2 Hz, 1H), 7.91-7.72 (2H, m, ArH), 7.67 (1H, t, *J* = 7.0 Hz, ArH), 7.50-7.40 (3H, m, ArH), 7.32-7.25 (1H, m, ArH), 4.83 (1H, s, 1/2ArCH$_2$N), 4.46 (1H, s, 1/2ArCH$_2$N), 4.36 (2H, s, ArCH$_2$), 3.88-3.49 (10H, m, 5CH$_2$), 2.80-2.66 (2H, m, NCH$_2$CH$_2$). ^{13}C-NMR (75 MHz, DMSO-d_6) δ (ppm): 169.7, 164.5, 164.2, 160.5, 159.4, 158.2, 154.9, 144.8, 140.7, 135.0, 133.4, 131.9, 131.5, 130.3, 129.1, 127.9, 126.1, 125.4, 123.8, 123.5, 121.1, 120.8, 116.1, 115.8, 113.4, 112.4, 66.0, 48.0, 46.6, 43.7, 36.5, 26.2. HRMS (ESI): m/z [M+H]$^+$. Calcd for $C_{34}H_{30}FN_8O_3$: 617.2419; Found: 617.2425. IR (cm^{-1}): 3424.49, 3244.90, 2893.88, 2853.06, 2360.47, 2341.85, 1654.10, 1560.94, 1541.11, 1494.69, 1493.03, 1410.32, 1354.44, 1265.51, 1226.68, 1111.29, 1017.85, 934.79, 845.15, 807.18, 783.57, 746.92.

4-(3-(2-(1H-indol-4-yl)-4-morpholino-5,6,7,8-tetrahydropyrido[3,4-d]pyrimidine-7-carbonyl)-4-fluorobenzyl)phthalazin-1(2*H*)-one (18). Off-white solid, 38% yield, m.p.: 178-180 ^{o}C. HPLC: 97.5%. ^{1}H NMR (300 MHz, DMSO-d_6) δ (ppm): 12.62 (1H, s, CONH), 11.29 (1H, s, NH), 8.26 (1H, t, *J* = 8.9 Hz, ArH), 8.12 (1H, d, *J* = 6.9 Hz, ArH), 8.02-7.74 (4H, m, ArH), 7.55-7.40 (4H, m, ArH), 7.34-7.14 (2H, m, ArH), 4.80 (1H, s, 1/2ArCH$_2$N), 4.45 (1H, s, 1/2ArCH$_2$N), 4.37 (2H, s, ArCH$_2$), 3.90-3.46 (10H, m, 5CH$_2$), 2.80-2.66 (2H, m, NCH$_2$CH$_2$). ^{13}C-NMR (75 MHz, DMSO-d_6) δ (ppm): 164.5, 164.1, 162.2, 160.2, 159.9, 159.4, 158.2, 151.5, 144.8, 140.7, 137.0, 134.9, 133.4, 132.0, 131.5, 129.1, 128.9, 127.9, 126.1, 125.4, 123.8, 120.4, 116.1, 115.9, 113.7, 112.6, 103.3, 66.1, 48.1, 46.6, 43.8, 36.5, 26.1. HRMS (ESI): m/z [M+H]$^+$. Calcd for $C_{35}H_{31}FN_7O_3$: 616.2467; Found: 616.2464. IR (cm^{-1}): 3421.58, 2895.18, 2851.32, 2360.36, 1647.20, 1563.27, 1493.88, 1438.70, 1405.72, 1341.95, 1302.71, 1264.90, 1227.21, 1203.52, 1164.82, 1110.89, 1066.37, 1048.46, 1014.57, 937.08, 847.38, 805.93, 763.57, 647.69, 557.44, 480.03.

In Vitro PARP Inhibition Assay. PARP-1 and PARP-2 inhibition assays were carried out

according to previously reported procedures.[42] The inhibition of the tested compounds on PARP-1 and PARP-2 enzymatic activity in a cell-free system was determined by ELISA in 96-well plates. Each well was pre-coated with histone (20 μg/mL) diluted in 100 μL of PBS buffer (10 mM NaH_2PO_4, 10 mM Na_2HPO_4, 150 mM NaCl, pH 7.4) and incubated at 37 °C overnight. After incubation, the plate was washed three times using 200 μL PBST buffer (1x PBS containing 0.05% (v/v) Tween 20) and blocked with 200 μL of Blocking buffer (1x PBST containing 5% (v/v) nonfat milk) at room temperature for 60 minutes. The plate was subsequently washed three times with 200 μL PBST buffer as described above. Then Biotinylated-NAD^+ (8 μM) and activator deoxyoligonucleotide (100 μg/mL) diluted in 70 μL of reaction buffer (50 mM Tris-HCl, 2 mM $MgCl_2$, pH 8.0) were added into each well, following by adding 10 μL of compound or solvent control at varying concentrations. Compounds to be tested were diluted in 10% (v/v) DMSO and tested in 10-dose with 3-fold serial dilution starting at a concentration of 1 μM. The reaction was initiated by the addition of 20 μL of PARP-1 or PARP-2 (10 ng/well) at 37 °C for 1 h. Discard the reaction mixture and wash plate three times with 200 μL PBST buffer and tap plate onto clean paper towel as described above. Add 50 μL of Streptavidin-HRP to each well. Incubate for 30 min at room temperature. Wash three times with 200 μL PBST buffer and tap plate onto clean paper towel as described above. Finally, 100 μL of ECL solution was added and incubated at room temperature for 15 min. Luminescent signal was measured using a multi-well spectrophotometer (Molecular Devices SpectraMax M5 microplate reader). The inhibition rate of PARP-1 or PARP-2 enzymatic activity was calculated as (Lu control − Lu treated/Lu control) × 100%. The concentration required for 50% inhibition of PARP-1 or PARP-2 enzymatic activity (IC_{50}) was calculated using nonlinear regression with normalized dose-response fit using Prism GraphPad software.

In Vitro PI3K Inhibition Assay. The assay was performed using ADP-Glo Plus luminescence kinase assay kit. 50 μL PI3K isoforms reaction mixture contains 10 mM Tris-HCl, pH 7.5, 25 μM ATP, 9.75 μM PIP2, 5% (v/v) glycerol, 4 mM $MgCl_2$, 50 mM NaCl, 0.05% (v/v) Chaps, 1 mM dithiothreitol, and 2% (v/v) DMSO at the following concentrations for each isoform: PI3Kα,β at 60 ng/mL; PI3Kγ at 8 ng/mL; PI3Kδ at 45 ng/mL. Compounds to be tested were diluted in 10% (v/v) DMSO and tested in 10-dose with 3-fold serial dilution starting at a concentration of 1 μM. The assay plate was covered and incubated at room temperature (PI3Kα, PI3Kβ, and PI3Kγ for 1 h and PI3Kδ for 2 h). Then, 50 μL ADP-Glo reagent was added and incubated for 40 min at room temperature followed by another 30 min incubation with 50 μL of kinase detection mixture. Luminescence signal was measured using a multi-well spectrophotometer (Molecular Devices SpectraMax M5 microplate reader). The IC_{50} values were calculated using nonlinear regression with normalized dose-response fit using Prism GraphPad software.

Cell Proliferation Inhibition Assay. The human-cancer-cell lines MDA-MB-231, MDA-MB-468, HCT116, HCC1937, BxPC-3, A2780, Jurkat, DU145, A549, Caki-1, Ramos and SW620 were maintained in RPMI1640 medium containing 10% (v/v) FBS at 37 °C in a 5% (v/v) CO_2 humidified incubator. Cell proliferation assay was determined by the Cell Titer-Glo cell viability assay. Briefly, cells were passaged the day before dosing into a 96-well plate, allowed to grow for 12 h, and then treated with different concentrations (see Table S2 for details) of compound for 7 days at 5% CO_2, 37°C. After incubation, 100 μL of Cell Titer-Glo reagent was added to the assay plate, which was then incubated at room temperature for 10 minutes to stabilize luminescence signal and read by Envision plate reader. The inhibition rate (%) = (1-(RLU compound－RLU blank) / (RLU DMSO

− RLU blank)) × 100%. The IC_{50} values were calculated using nonlinear regression with normalized dose-response fit using XLFit software.

Western Blot Assay. MDA-MB-468 cells were seeded into six-well plates and incubated overnight and then treated with or without different concentrations of compounds (BKM120 (1 μM), Olaparib (2 μM), BKM120 (1 μM) + Olaparib (2 μM), **14** (1 μM) and **15** (1 μM) for 6 h, medium with 1‰ (v/v) DMSO was used as the control. Cell samples were collected in ice-cold lysis buffer. Lysates were cleared by centrifugation at 14,000 rpm for 10 minutes at 4 ^{o}C, and supernatants were removed and assayed for protein concentration using the Pierce BCA Protein Assay Kit (Thermo Scientific). Cell lysates were loaded to 8-12% SDS-PAGE and separated by electrophoresis. Separated proteins were then electrically transferred to polyvinylidene difluoride membranes (Millipore), which were blocked with 5% bovine serum albumin/TBST for 1 h. Membranes were hybridized with the following primary antibodies: phospho-AKT (pAKT-Ser473), total AKT, phospho-S6 (pS6-Ser240), total S6, phospho-ERK (pERK-Thr202), total ERK, phospho-ETS1 (pETS1-Thr38), total ETS1, BRCA1, BRCA2, cleaved PARP (Abcam) and β-actin (Abcam) in 1% nonfat dry milk. The bands were visualized using enhanced chemiluminescence (Thermo Scientific) after hybridization with a HRP-conjugated secondary antibody and then quantified by ImageJ software.

Real-time PCR. The relative expression of BRCA1 or BRCA2 mRNA was detected using Real-time PCR. Briefly, total RNA was extracted from cultured cells with TRIzol reagent (Life Technologies) according to the manufacturers' instructions. Reverse transcription reactions were performed using PrimeScript™ RT reagent Kit with gDNA Eraser (Takara). For transcript quantification, SYBR Green based qPCR was performed with PrimeScript™ RT Master Mix

(Takara) using Real Time PCR System (Stratagene Mx3000p). The human BRCA1 forward primer was 5'-GTCCCATCTGTCTGGAGTTGA-3', the reverse primer was 5'-AAAGGACACTGTGAAGGCCC-3'. The human BRCA2 forward primer was 5'-AAAGGACACTGTGAAGGCCC-3', and the reverse primer was 5'-TTCTTCCTCTCTTTCATTGCG-3'. GAPDH was used as an internal control. The results were represented as fold changes relative to the internal control.

Immunofluorescence Staining. MDA-MB-468 cells were cultured on coverslips in 24-well plates in respective medium containing different drugs for 72 h. Three days after drugs treatment, the cells were fixed with 3% formaldehyde, permeabilized with 0.1% Triton X-100, and blocked with 10% FBS-containing PBS medium for 1 hour. Subsequently, cells were incubated with rabbit anti-RAD51 polyclonal antibody (Santa Cruz Biotechnology) or rabbit anti-γH2AX (Ser139) polyclonal antibody (Cell Signaling Technology) overnight at 4 ^{o}C. After overnight staining, cells were washed three times with PBS, subsequently blocked for 30 min, and then incubated with secondary antibodies for 2 hours and DAPI for 30 min at room temperature protected from light. Lastly, cells were washed three times with PBS, and then mounted in anti-fade mounting medium. Images were acquired and quantified using an immunofluorescence microscope (Leica). The foci accumulation of phosphorylated histone H2AX (γH2AX) and RAD51, as well as percentage of positive cells (more than 5 foci in one cell) were calculated based on analysis of about 200 cells.

Comet Assay. Cells were treated and harvested after drugs treatment for 72 h, and subjected to the neutral comet assay. Following electrophoresis, the cells were stained with ethidium bromide. We analyzed about 200 individual cell images from each group using Comet Assay Software Pect

(CaspLab) software. Tail intensity (percentage DNA in the tail) was defined and served as a quantitative measure of DNA damage.

In Vivo Antitumor Activity Study. Six-week-old male BALB/c nude mice were purchased from the Beijing Vital River Laboratory Animal Technology Co., Ltd. All animals were housed in a specific pathogen-free facility and used according to the animal-care regulations of Nanjing Biorn Life Science Co., Ltd (Nanjing, Jiangsu, China). The animal permit number is SCXK (Peking) 2016-0011. Prior to implantation, MDA-MB-468 cells were harvested during exponential growth. 2×10^6 cells were inoculated subcutaneously on the right flank of each BALB/c nude mouse. Mice were randomly divided into five treatment groups and control group when tumor size reached an approximate volume of 100 mm^3. Olaparib (50 $mg\cdot kg^{-1}$), BKM120 (27.5 $mg\cdot kg^{-1}$), Olaparib + BKM120 (50 $mg\cdot kg^{-1}$ + 27.5 $mg\cdot kg^{-1}$), **14** (50 $mg\cdot kg^{-1}$) and **15** (50 $mg\cdot kg^{-1}$) was administered every 2 days for 34 days (6 mice per group) by intraperitoneal administration, The treatment with equal volume of PBS (5% DMSO, v/v) was used as the negative control. During treatment, tumor size and body weight were measured every 2 days Tumor volume (V) was calculated using the equation $V = ab^2/2$, where *a* and *b* stand for the longest and shortest diameter measured by vernier caliper, respectively.

Molecular Modeling. The X-ray crystal structures of PARP-1 (PDB ID: 5DS3) and PI3Kα (PDB ID: 4JPS) were retrieved from the Protein Data Bank. The protein structures were prepared using Protein Preparation Wizard module. Hydrogen atoms were added, water molecules in all the system were removed, followed by energy minimization and optimization by OPLS_2005 force field. Grids of PARP-1 and PI3Kα were generated using Glide, version 10.2, following the standard procedure recommended by Schrodinger (Cambridge, MA). Ligand Preparation Wizard module

was employed to prepare the compounds for molecular docking. To prepare ligand structures, hydrogens were added, 3D geometries, ionization and tautomeric states were generated. Finally, the ligand structures were minimized using OPLS 2005 force field. The conformational ensembles were docked flexibly using Glide with the standard settings in both the standard and extra-precision modes. Only poses with low energy conformations and good hydrogen-bond geometries were considered.

ASSOCIATED CONTENT

Supporting Information

The Supporting Information is available free of charge on the ACS Publications website at DOI:

Binding Mode Analysis of Olaparib and BKM120 (Figure S1 and S2) (PDF)

Specific Data of Kinase Profiling of Compound **15** (Table S1) (PDF)

^{1}H NMR and ^{13}C NMR spectra of all target compounds (PDF)

Molecular formula strings and some data (CSV)

Accession Codes

PDB code 5DS3 was used for modeling docking of compound **1** in PARP-1; PDB code 4JPS was used for modeling docking of compound **1** in PI3Kα.

AUTHOR INFORMATION

Corresponding Author

*Y.X: phone: (86)-25-83271244. E-mail: xyg@cpu.edu.cn.

*Q.Z: phone: (86)-25-83271244. E-mail: zhuqihua@vip.126.com.

Notes

The authors declare no competing financial interest

ACKNOWLEDGMENTS

This work was supported by the National Natural Science Foundation of China (Grant No. 81502928) and Outstanding Scientific and Technological Innovation Team Projects of Jiangsu Province, China (2015).

ABBREVIATIONS USED

PARP, poly(ADP-ribose)polymerase; PI3K, phosphoinositide 3-kinase; NAD^+, nicotinamide adenine dinucleotide; SSBs, single strand breaks; SL, synthetic lethal; DSBs, double-strand breaks; HR, homologous recombination; TNBC, triple-negative breast cancer; ERK, extracellular regulated protein kinase; AKT, protein kinase B; S6, ribosomal protein S6 kinase; PCR, polymerase chain reaction; TGI, tumor growth inhibition; SAR, structure-activity relationship; DIPEA, *N,N*-diisopropylethylamine; EtOAc, ethyl acetate; DMF, *N,N*-dimethylformamide; DCM, dimethyl chloride; DMSO, dimethyl sulfoxide; PyBOP, benzotriazol-1-yl-oxytripyrrolidinophosphonium hexafluorophosphate; TLC, thin-layer chromatography

REFERENCES

(1) Hanahan, D.; Weinberg, R. A. Hallmarks of cancer: the next generation. *Cell* **2011**, *144*, 646−674.

(2) Stewart, B. W.; Wild, C. P. *World Cancer Report 2014.* International Agency for Research on Cancer, Lyon. **2014**.

(3) Anighoro, A.; Bajorath, J.; Rastelli, G. Polypharmacology: challenges and opportunities in drug discovery: miniperspective. *J. Med. Chem.* **2014**, *57*, 7874−7887.

(4) Peters, J.-U. Polypharmacology−foe or friend? *J. Med. Chem.* **2013**, *56*, 8955−8971.

(5) Morphy, R.; Rankovic, Z. Designed multiple ligands. an emerging drug discovery paradigm. *J. Med. Chem.* **2005**, 48, 6523−6543.

(6) O'Boyle, N. M.; Meegan, M. J. Designed multiple ligands for cancer therapy. *Curr. Med. Chem.* **2011**, *18*, 4722−4737

(7) Schreiber, V.; Dantzer, F.; Ame, J. C.; de Murcia, G. Poly(ADP-ribose): Novel functions for an old molecule. *Nat. Rev. Mol. Cell Biol.* **2006**, *7*, 517–528.

(8) Wang, Y. Q.; Wang, P. Y.; Wang, Y. T.; Yang, G. F.; Zhang, A.;, Miao, Z. H. An update on poly(ADP-ribose)polymerase-1 (PARP-1) inhibitors: opportunities and challenges in cancer therapy. *J. Med. Chem.* **2016**, *59*, 9575−9598.

(9) Rouleau, M.; Patel, A.; Hendzel, M. J.; Kaufmann, S. H.; Poirier, G. G. PARP inhibition: PARP1 and beyond. *Nat. Rev. Cancer* **2010**, *10*, 293-301.

(10) Ferraris, D. V. Evolution of poly(ADP-ribose) polymerase-1 (PARP-1) inhibitors. From concepts to clinic. *J. Med. Chem.* **2010**, *53*, 4561−4584.

(11) Yelamos, J.; Farres, J.; Lacuna, L.; Ampurdanes, C.; MartinCaballero, J. PARP-1 and PARP-2: new players in tumour development. *Am. J. Cancer Res.* **2011**, *1*, 328−346.

(12) Pommier, Y.; O'Connor, Mark. J.; Bono, J. D. Laying a trap to kill cancer cells: PARP inhibitors and their mechanisms of action. *Sci. Transl. Med.* **2016**, *8*, 362ps17.

(13) Dréan, A.; Lord, C. J.; Ashworth, A. PARP inhibitor combination therapy. *Crit. Rev. Oncol. Hematol.* **2016**, *108*, 73–85.

(14) Purnell, M. R.; Whish, W. J. Novel inhibitors of poly(ADP-ribose) synthetase. *Biochem. J.* **1980**, *185*, 775–777.

(15) Bryant, H. E.; Schultz, N.; Thomas, H. D.; Parker, K. M.; Flower, D.; Lopez, E.; Kyle, S.; Meuth, M.; Curtin, N. J.; Helleday, T. Specific killing of BRCA2-deficient tumours with inhibitors of poly(ADP-ribose) polymerase. *Nature* **2005**, *434*, 913−917.

(16) Farmer, H.; McCabe, N.; Lord, C. J.; Tutt, A. N.; Johnson, D. A.; Richardson, T. B.; Santarosa, M.; Dillon, K. J.; Hickson, I.; Knights, C.; Martin, N. M.; Jackson, S. P.; Smith, G. C.; Ashworth, A. Targeting the DNA repair defect in BRCA mutant cells as a therapeutic strategy. *Nature* **2005**, *434*, 917–921.

(17) Morales, J.; Li, L.; Fattah, F. J.; Dong, Y.; Bey, E. A.; Patel, M.; Gao, J.; Boothman, D. A. Review of poly (ADP-ribose) polymerase (PARP) mechanisms of action and rationale for targeting in cancer and other diseases. *Crit. Rev. Eukaryotic Gene Expression* **2014**, *24*, 15−28.

(18) Lord, C. J.; Ashworth, A. PARP inhibitors: Synthetic lethality in the clinic. *Science* **2017**, *355*, 1152–1158.

(19) Menear, K. A.; Adcock, C.; Boulter, R.; Cockcroft, X. L.; Copsey, L.; Cranston, A.; Dillon, K. J.; Drzewiecki, J.; Garman, S.; Gomez, S.; Javaid, H.; Kerrigan, F.; Knights, C.; Lau, A.; Loh, V. M., Jr.; Matthews, I. T.; Moore, S.; O'Connor, M. J.; Smith, G. C.; Martin, N. M. 4-[3-(4-Cyclopropanecarbonylpiperazine-1-carbonyl)-4-fluorobenzyl]-2H-phthalazin-1-one: a novel bioavailable inhibitor of poly-(ADP-ribose) polymerase-1. *J. Med. Chem.* **2008**, *51*, 6581−6591.

(20) Thomas, H. D.; Calabrese, C. R.; Batey, M. A.; Canan, S.; Hostomsky, Z.; Kyle, S.; Maegley,

K. A.; Newell, D. R.; Skalitzky, D.; Wang, L. Z.; Webber, S. E.; Curtin, N. J. Preclinical selection of a novel poly(ADP-ribose) polymerase inhibitor for clinical trial. *Mol. Cancer Ther.* **2007**, *6*, 945−956

(21) (a) Jones, P.; Altamura, S.; Boueres, J.; Ferrigno, F.; Fonsi, M.; Giomini, C.; Lamartina, S.; Monteagudo, E.; Ontoria, J. M.; Orsale, M. V.; Palumbi, M. C.; Pesci, S.; Roscilli, G.; Scarpelli, R.; SchultzFademrecht, C.; Toniatti, C.; Rowley, M. Discovery of 2-{4-[(3S)-piperidin-3-yl]phenyl}-2H-indazole-7-carboxamide (MK-4827): a novel oral poly(ADP-ribose) polymerase (PARP) inhibitor efficacious in BRCA-1 and −2 mutant tumors. *J. Med. Chem.* **2009**, *52*, 7170−7185. (b) Jones, P.; Wilcoxen, K.; Rowley, M.; Toniatti, C. Niraparib: a poly(ADP-ribose) polymerase (PARP) inhibitor for the treatment of tumors with defective homologous recombination. *J. Med. Chem.* **2015**, *58*, 3302−3314.

(22) Wang, B.; Chu, D.; Feng, Y.; Shen, Y.; Aoyagi-Scharber, M.; Post, L. E. Discovery and characterization of (8S, 9R)-5-fluoro-8-(4-fluorophenyl)-9-(1-methyl-1H-1, 2, 4-triazol-5-yl)-2, 7, 8, 9-tetrahydro-3H-pyrido [4, 3, 2-de] phthalazin-3-one (BMN 673, talazoparib), a novel, highly potent, and orally efficacious poly (ADP-ribose) polymerase-1/2 inhibitor as an anticancer agent. *J. Med. Chem.* **2016**, *59*, 335−357.

(23) Penning, T. D.; Zhu, G. D.; Gandhi, V. B.; Gong, J.; Liu, X.; Shi, Y.; Klinghofer, V.; Johnson, E. F.; Donawho, C. K.; Frost, D. J.; Bontcheva-Diaz, V.; Bouska, J. J.; Osterling, D. J.; Olson, A. M.; Marsh, K. C.; Luo, Y.; Giranda, V. L. Discovery of the poly-(ADP-ribose) polymerase (PARP) inhibitor 2-[(R)-2-methylpyrrolidin-2-yl]-1H-benzimidazole-4-carboxamide (ABT-888) for the treatment of cancer. *J. Med. Chem.* **2009**, *52*, 514−523.

(24) Ferraris, D. V. Evolution of poly(ADP-ribose) polymerase-1 (PARP-1) inhibitors. From

concept to clinic. *J. Med. Chem.* **2010**, *53*, 4561−4584.

(25) Benafif, S.; Hall, M. An update on PARP inhibitors for the treatment of cancer. *OncoTargets Ther.* **2015**, *8*, 519−528.

(26) Wong, K. K.; Engelman, J. A.; Cantley, L. C. Targeting the PI3K signaling pathway in cancer. *Curr. Opin. Genet. Dev.* **2010**, *20*, 87–90.

(27) Fruman, D. A.; Rommel, C . PI3K and cancer: lessons, challenges and opportunities. *Nat. Rev. Drug Discov.* **2014**, 13, 140–156.

(28) Kumar, A.; Fernandez-Capetillo, O.; Carrera, A. C. Nuclear phosphoinositide 3-kinase beta controls double-strand break DNA repair. *Proc. Natl. Acad. Sci. U. S. A.* **2011**, *107*, 7491-7496.

(29) Kao, G. D.; Jiang, Z.; Fernandes, A. M.; Gupta, A. K.; Maity, A. Inhibition of phosphatidylinositol-3-OH kinase/Akt signaling impairs DNA repair in glioblastoma cells following ionizing radiation. *J. Biol. Chem.* **2007**, *282*, 21206–21212.

(30) Ibrahim, Y. H.; Garcia-Garcia, C.; Serra, V.; He, L.; Torres-Lockhart, K.; Prat, A.; Anton, P.; Cozar, P.; Guzmán, M.; Grueso, J.; Rodríguez, O.; Calvo, M. T.; Aura, C.; Díez, O.; Rubio, I. T.; Pérez, J.; Rodón, J.; Cortés, J.; Ellisen, L. W.; Scaltriti, M.; Baselga, J. PI3K inhibition impairs BRCA1/2 expression and sensitizes BRCA-profcient triple-negative breast cancer to PARP inhibition. *Cancer Discov.* **2012**, 2, 1036–1047.

(31) Juvekar, A.; Burga, L. N.; Hu, H.; Lunsford, E. P.; Ibrahim, Y. H.; Balmañà, J.; Rajendran, A.; Papa, A.; Spencer, K.; Lyssiotis, C. A.; Nardella, C.; Pandolfi, P. P.; Baselga, J.; Scully, R.; Asara, J. M.; Cantley, L. C.; Wulf, G. M. Combining a PI3K inhibitor with a PARP inhibitor provides an effective therapy for BRCA1-related breast cancer. *Cancer Discov.* **2012**, *2*, 1048–1063.

(32) Matulonis, U. A.; Wulf, G. M.; Barry, W. T.; Birrer, M.; Westin, S. N.; Farooq, S.; Bell-

McGuinn, K. M.; Obermayer, E.; Whalen, C.; Spagnoletti, T.; Luo, W.; Liu, H.; Hok, R. C.; Aghajanian, C.; Solit, D. B.; Mills, G. B.; Taylor, B. S.; Won, H.; Berger, M. F.; Palakurthi, S.; Liu, J.; Cantley, L. C.; Winer, E. Phase I dose escalation study of the PI3kinase pathway inhibitor BKM120 and the oral poly (ADP ribose) polymerase (PARP) inhibitor olaparib for the treatment of high grade serous ovarian and breast cancer. *Ann. Oncol.* **2017**, 28, 512–518.

(33) Burger, M. T.; Pecchi, S.; Wagman, A.; Ni, Z. J.; Knapp, M.; Hendrickson, T.; Atallah, G.; Pfister, K.; Zhang, Y.; Bartulis, S.; Frazier, K.; Ng, S.; Smith, A.; Verhagen, J.; Haznedar, J.; Huh, K.; Iwanowicz, E.; Xin, X.; Menezes, D.; Merritt, H.; Lee, I.; Wiesmann, M.; Kaufman, S.; Crawford, K.; Chin, M.; Bussiere, D.; Shoemaker, K.; Zaror, I.; Maira, S. M.; Voliva, C. F. Identification of NVP-BKM120 as a potent, selective, orally bioavailable class I PI3 kinase inhibitor for treating cancer. *ACS Med. Chem. Lett.* **2011**, *2*, 774–779.

(34) Dawicki-McKenna, J. M.; Langelier, M. F.; DeNizio, J. E.; Riccio, A. A.; Cao, C. D.; Karch, K. R.; McCauley, M.; Steffen, J. D.; Black, B. E.; Pascal, J. M. PARP-1 activation requires local unfolding of an autoinhibitory domain. *Mol. Cell* **2015**, *60*, 755−768.

(35) Reilly, S. W.; Puentes, L. N.; Wilson, K.; Hsieh, C. J.; Weng, C. C.; Makvandi, M.; Mach, R. H. Examination of diazaspiro cores as piperazine bioisosteres in the olaparib framework shows reduced DNA damage and cytotoxicity. *J. Med. Chem.* **2018**, *61*, 5367−5379.

(36) Wang, Y. Q.; Wang, P. Y.; Wang, Y. T.; Yang, G. F.; Zhang, A.; Miao, Z. H. An Update on poly(ADP-ribose)polymerase-1 (PARP-1) inhibitors: opportunities and challenges in cancer therapy. *J. Med. Chem.* **2016**, *59*, 9575−9598.

(37) Thorsell, A. G.; Ekblad, T.; Karlberg, T.; Low, M.; Pinto, A. F.; Tresaugues, L.; Moche, M.; Cohen, M. S.; Schuler, H. Structural basis for potency and promiscuity in poly(ADP-ribose)

polymerase (PARP) and tankyrase inhibitors. *J. Med. Chem.* **2017**, *60*, 1262–1271.

(38) Maira, S. M.; Pecchi, S.; Huang, A.; Burger, M.; Knapp, M.; Sterker, D.; Schnell, C.; Guthy, D.; Nagel, T.; Wiesmann, M.; Brachmann, S.; Fritsch, C.; Dorsch, M.; Chene, P.; Shoemaker, K.; De Pover, A.; Menezes, D.; Martiny-Baron, G.; Fabbro, D.; Wilson, C. J.; Schlegel, R.; Hofmann, F.; Garcia-Echeverria, C.; Sellers, W. R.; Voliva, C. F. Identification and characterization of NVP-BKM120, an orally available pan-class I PI3-kinase inhibitor. *Mol. Cancer Ther.* **2012**, *11*, 317–328.

(39) Maira, S. M.; Pecchi, S.; Huang, A.; Burger, M.; Knapp, M.; Sterker, D.; Schnell, C.; Guthy, D.; Nagel, T.; Wiesmann, M.; Brachmann, S.; Fritsch, C.; Dorsch, M.; Chene, P.; Shoemaker, K.; De Pover, A.; Menezes, D.; Martiny-Baron, G.; Fabbro, D.; Wilson, C. J.; Schlegel, R.; Hofmann, F.; Garcia-Echeverria, C.; Sellers, W. R.; Voliva, C. F. Identification and characterization of NVP-BKM120, an orally available pan-class I PI3-kinase inhibitor. *Mol. Cancer Ther.* **2012**, *11*, 317−328.

(40) Sutherlin, D. P.; Bao, L.; Berry, M.; Castanedo, G.; Chuckowree, I.; Dotson, J.; Folks, A.; Friedman, L.; Goldsmith, R.; Gunzner, J.; Heffron, T.; Lesnick, J.; Lewis, C.; Mathieu, S.; Murray, J.; Nonomiya, J.; Pang, J.; Pegg, N.; Prior, W. W.; Rouge, L.; Salphati, L.; Sampath, D.; Tian, Q.; Tsui, V.; Wan, N. C.; Wang, S.; Wei, B.; Wiesmann, C.; Wu, P.; Zhu, B. Y.; Olivero, A. Discovery of a potent, selective, and orally available class I phosphatidylinositol 3-kinase (PI3K)/mammalian target of rapamycin (mTOR) kinase inhibitor (GDC-0980) for the treatment of cancer. *J. Med. Chem.* **2011**, *54*, 7579–7587.

(41) Folkes, A. J.; Ahmadi, K.; Alderton, W. K.; Alix, S.; Baker, S. J.; Box, G.; Chuckowree, I. S.; Clarke, P. A.; Depledge, P.; Eccles, S. A.; Friedman, L. S.; Hayes, A.; Hancox, T. C.; Kugendradas, A.; Lensun, L.; Moore, P.; Olivero, A. G.; Pang, J.; Patel, S.; Pergl-Wilson, G. H.; Raynaud, F. I.;

Robson, A.; Saghir, N.; Salphati, L.; Sohal, S.; Ultsch, M. H.; Valenti, M.; Wallweber, H. J.; Wan, N. C.; Wiesmann, C.; Workman, P.; Zhyvoloup, A.; Zvelebil, M. J.; Shuttleworth, S. J. The identification of 2-(1H-indazol-4-yl)-6-(4-methanesulfonyl-piperazin-1-ylmethyl)-4-morpholin-4-yl-thieno[3,2-d]pyrimidine (GDC-0941) as a potent, selective, orally bioavailable inhibitor of class I PI3 kinase for the treatment of cancer. *J. Med. Chem.* **2008**, *51*, 5522–5532.

(42) Ye, N.; Chen, C. H.; Chen, T.; Song, Z.; He, J. X.; Huan, X. J.; Song, S. S.; Liu, Q.; Chen, Y.; Ding, J.; Xu, Y.; Miao, Z. H.; Zhang, A. Design, synthesis, and biological evaluation of a series of benzo[*de*][1,7]naphthyridin-7(8*H*)-ones bearing a functionalized longer chain appendage as novel PARP1 inhibitors. *J. Med. Chem.* **2013**, *56*, 2885–2903.

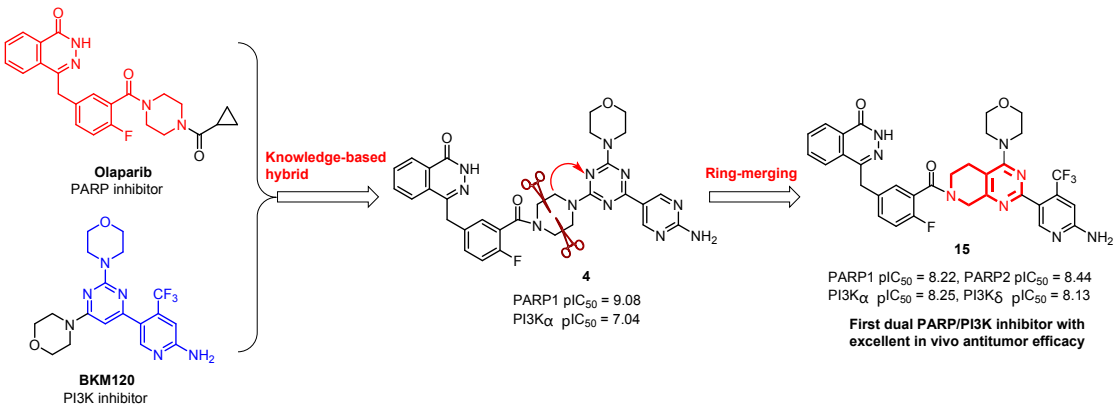
Olaparib
PARP inhibitor
BKM120
PI3K inhibitor
Knowledge-based hybrid
4
PARP1 pIC50 = 9.08
PI3Kα pIC50 = 7.04
Ring-merging
15
PARP1 pIC50 = 8.22, PARP2 pIC50 = 8.44
PI3Kα pIC50 = 8.25, PI3Kδ pIC50 = 8.13
First dual PARP/PI3K inhibitor with excellent in vivo antitumor efficacy